

Coaxing the Eclipsing Binary V367 Cygni Out of its Shell

T.J. Davidge^{1,2}

*Dominion Astrophysical Observatory,
Herzberg Astronomy & Astrophysics Research Center,
National Research Council of Canada, 5071 West Saanich Road,
Victoria, BC Canada V9E 2E7
tim.davidge@nrc.ca; tdavidge1450@gmail.com*

ABSTRACT

Spectra that cover $0.63 - 0.69\mu\text{m}$ with a spectral resolution ~ 17000 are presented of the W Serpentis system V367 Cygni. Absorption lines of FeII and SiII that form in a circumsystem shell are prominent features, and the depths of these are stable with time, suggesting that the shell is smoothly distributed and well-mixed. Further evidence of uniformity comes from modest radial velocity variations measured in the deepest parts of the shell lines. It is suggested that motions previously attributed to rotation of the shell are instead artifacts of contamination from the donor star spectrum. A donor star spectrum is extracted that is consistent with that of an early to mid-A giant. The depths of metallic lines in the donor spectrum vary with orbital phase, suggesting that spot activity covers a large fraction of the surface of that star. A spectrum of the accretion disk that surrounds the second star is also extracted, and similarities are noted with the emission spectra of Herbig Ae/Be stars. In addition to variations with orbital phase, H α changes with time over timescales of no more than two orbits. A tentative detection of HeI 6678 emission is made near primary minimum, but not at other phases. Finally, projected emission from hot dust in and around V367 Cyg is more-or-less symmetric and extends over 28 arcsec, or 0.09 pc at the distance of the system – V367 Cyg is thus expelling matter into a large volume of the surrounding space.

¹Based on observations obtained at the Dominion Astrophysical Observatory, Herzberg Astronomy and Astrophysics Research Centre, National Research Council of Canada.

²This research has made use of the NASA/IPAC Infrared Science Archive, which is funded by the National Aeronautics and Space Administration and operated by the California Institute of Technology.

1. INTRODUCTION

Many stars in the solar neighborhood are in binary systems (e.g. Abt 1983). If the stars are close enough together then mass will be transferred between components. Initially, material from the more massive star is transferred to the lower mass star as evolution causes the former to expand and fill its Roche lobe. An additional exchange of mass may occur when the star that accretes this material evolves.

The transfer of mass and angular momentum in such close binary systems (CBSs) causes the evolution of both components to depart from that of single stars, and this has potential implications for a range of astrophysical topics. Departures from single star evolution are expected to be common among massive stars, as the binary frequency among these objects is high (Sana et al. 2012). Such interactions in massive CBSs can skew population statistics in studies of the stellar contents of other galaxies (De Mink et al. 2014), and it has been suggested that some of the brightest objects in star-forming galaxies, such as luminous blue variables and supergiant B[e] stars, may be CBSs (e.g. Smith & Tombleson 2015; Clark et al. 2013). Mass transfer can also affect the properties of the compact objects that are the end products of massive star evolution (e.g. Ertl et al. 2020).

As with massive stars, a significant population of intermediate mass stars are likely in CBSs. Semi-detached (SD) systems, in which one star fills its Roche lobe, are common among eclipsing binaries that contain intermediate mass stars (e.g. Malkov 2020). Given that eclipsing systems sample a restricted range of orbital orientations then the number of as yet undetected intermediate mass SD systems will be even higher than in the Malkov (2020) census. One implication is that binary white dwarf (WD) systems, which are one possible end point of CBS evolution involving intermediate mass stars, may not be rare.

Systems that are in the early stages of interaction are of particular interest as the component stars are closer to their original states than in more evolved systems. Such systems thus require fewer assumptions about the nature of the progenitor stars when making comparisons with models. That being said, the rate of mass transfer is highest at these times, as evolution forces the donor star to expand into its Roche lobe and the separation between components decreases prior to the reversal of the mass ratio. The rapid early evolution of these systems can complicate efforts to understand the system properties, as an accretion disk around the accreting star may block light from that object, while a circumsystem shell may complicate efforts to detect the spectra of both components. Models of CBSs discussed by Nelson & Eggleton (2001) predict a large initial spike in mass transfer rates over a dynamical timescale, followed by a mass transfer rate that is ~ 2 orders of magnitude lower than the peak value.

W Serpentis (W Ser) is an enigmatic CBS that is the archetype of a group first discussed by Plavec & Koch (1978). Aside from binarity, a defining characteristic of this group is a UV spectrum that is indicative of excitation levels that can not be attributed to the component stars. There are also photometric and spectroscopic properties that are suggestive of large scale mass transfer. β Lyrae is likely the nearest W Ser system, and interferometric observations discussed by Zhao et al. (2008) reveal the distorted nature of its components.

W Ser systems are thought to be in the early phases of mass transfer. The stream of matter from the donor star forms an accretion disk. A hot spot may then form where the stream impacts the disk, and this spot can affect the observational properties of the system. Table 1 of Van Rensbergen et al. (2011) lists spot temperatures in selected W Ser systems, and spots with temperatures in excess of 20000K are common. Hot spots thus provide a plausible source of the high energies needed to power UV emission. Variations in the spot brightness and location may also affect the photometric properties of W Ser systems at visible wavelengths.

Only a modest number of W Ser systems have been identified to date, and the majority of these are located within ~ 1 kpc (e.g. Elias 1990). The small number of confirmed systems is in part a selection effect, as there is a bias towards eclipsing systems (i.e. those with orbital inclinations in excess of $\sim 65^\circ$). There are undoubtedly non-eclipsing W Ser systems located within 1 kpc that remain to be identified or that have an uncertain classification.

In the current paper we examine the spectroscopic properties of V367 Cyg, which is one of the five systems discussed by Plavec & Koch (1978). The parallax of V367 Cyg listed in the GAIA Data Release 2 (Brown et al. 2018) is 1.05 marcsec, indicating a distance of 670 parsecs.¹ Models examined by Van Rensbergen et al. (2011) suggest that V367 Cyg is likely undergoing Case B mass transfer given its orbital period of 18.6 days. UV emission line strengths suggest that processed material has not yet been accessed in the donor star (Plavec et al. 1984).

The broad-band spectral energy distribution (SED) of V367 Cyg provides basic limits on the effective temperatures of the system components. Based on a single low resolution spectrum although this classification was undoubtedly influenced by shell lines, and so does not reflect the actual spectral types of the component stars. The UV continuum is consistent with sources that have effective temperatures of 8000 and 10000K (Hack et al. 1984), while the SED between 1 and $2.5\mu\text{m}$ is indicative of components that have effective temperatures of 9000 and 11000 K (Taranova & Shenavrin 2005). The temperatures found from the UV and

¹This distance has not been corrected for possible systematic effects in the parallax measurements, such as zeropoint offsets (e.g. Lindgren et al. 2018).

IR data thus suggest that the dominant components have SEDs that are consistent with late B/early A to mid-A spectral types. Still, the light from the accreting star may be masked by an accretion disk. Moreover, at longer wavelengths the SED contains excess infrared (IR) emission (Taranova 1997, Taranova & Shenavrin 2005), indicating a non-stellar contribution to the SED. The IR properties are similar to those of β Lyrae (Taranova & Shenavrin 2005), although there are differences at radio wavelengths (Elias 1990).

It has been known for some time that the dominant absorption lines in the spectrum of V367 Cyg at visible wavelengths originate in a circumsystem shell (e.g. Abt 1954; Heiser 1961 and references therein). The shell lines at wavelengths $< 5000\text{\AA}$ tend to have similar kinematic behaviours, although there are exceptions (Aydin et al. 1978; Hack et al. 1984) that have been attributed to ejection events (Hack et al. 1984). The profiles of the shell line vary with orbital phase, and this has been linked to possible non-uniform shell structure (Abt 1954, Heiser 1961, Aydin et al. 1978). Variations related to ionization are also present that are suggestive of stratification (Aydin et al. 1978). Hack et al. (1984) estimate a shell mass of 10^{-5} to $10^{-6} M_{\odot}$.

Absorption lines in the spectrum of the donor star have been detected in previous studies, although veiling by the shell, coupled with line broadening due to the donor’s rotation, complicate efforts to detect these lines. Even though shell lines may mask the donor spectrum, lines from the donor can still be untangled from shell lines given that the orbital velocity of the donor differs markedly from that of the shell (Section 5). While high order Balmer lines and Ca H and K show evidence of a contribution from the donor star (Heiser 1961, Aydin et al. 1978), past attempts to examine the properties of the donor star have largely focused on MgII 4481.

Despite extensive searches, no spectroscopic signatures of the accreting star have been found (Schneider et al. 1993). This is perhaps not surprising, as the accreting star is intrinsically fainter than the more evolved donor, and an accretion disk may mask much of its light. V367 Cyg is thus a single line spectroscopic binary, and so the masses of the component stars are uncertain. This uncertainty is reflected in the published mass estimates, which are summarized in Table 1. The uncertainties in this table are from the source papers, when available. There is considerable dispersion among the entries, highlighting the uncertain nature of V367 Cyg and its eventual end state.

While the detection of spectroscopic signatures from the accreting star is problematic, there are other potential tracers of its orbital motion. For example, given a possible association with the hot spot, UV emission lines might probe the dynamical properties of the accretor and the surrounding disk, including the escape velocity (Deschamps et al. 2015). Tarasov & Berdyugin (1998) discuss the possible detection of HeI 6678 emission, pointing

Donor (M_{\odot})	Accretor (M_{\odot})	Source	Method ^a
6.7	6.7	Aydin et al. (1978)	RVs without disk; mass ratio fixed
19 ± 4	12 ± 3	Li & Leung (1987)	LC fitting without disk; no RVs
4.4	2.5	Pavlovski et al. (1992)	LC+RVs; with disk
22	11	Tarasov & Berdyugin (1998)	LC+RV of accretor based on HeI 6678
21.7 ± 2.8	11.0 ± 0.8	Zola & Ogloza (2001)	LC without disk; $l_3 = 0$
3.3 ± 0.9	4.0 ± 0.5	Zola & Ogloza (2001)	LC with disk; $l_3 = 0$

Table 1: Mass estimates

^aRV = radial velocity; LC = light curve; l_3 = third light

out that it defines a velocity curve that is out of phase with that of the donor. They argue that the line originates in the accretion disk that surrounds the accreting star, and use it to trace the orbital motion of the latter. The detection of HeI 6678 has been challenged by Zola & Ogloza (2001), who note that the detected feature is in a complex mix of shell lines, making its identification uncertain.

Additional uncertainties in the nature of the stars in V367 Cyg result from the complicated nature of the light curve. The light curves of W Ser systems tend to have a unequal maxima. This is not a rare phenomenon among CBSs (e.g. O’Connell 1951, Milone 1968, Davidge & Milone 1984), and there are indications that there is more than one cause (e.g. Davidge & Milone 1984). The differences between the out-of-eclipse maxima in W Ser systems tend to vary over time scales of many orbital cycles, and this is also the case in the V367 Cyg light curve. Such variations highlight the non-uniform distribution of light-emitting regions in the system, likely due in part to the accretion hot spot and possible activity on the donor star. Such photometric irregularities complicate light curve analysis.

The accretion disk is a significant source of light in V367 Cyg that must be considered in light curve models. Perhaps the most direct approach is to consider the accreting star and its accompanying disk as a single star-like body (i.e. assume that the disk hugs the surface of the accreting star). Solely in terms of light output this is not a bad assumption, as the accreting star may be completely shielded by the disk. However, the shape of a rapidly rotating disk will almost certainly differ from that of a star, compromising the physical interpretation of parameters estimated from the light curve. Li & Leung (1987) and Zola & Ogloza (2001) examine such models and find that the donor star and the other body are in, or are close to, contact with their Roche surfaces. An inspection of Table 1 indicates that

these light curve solutions also tend to predict component masses that are at the upper end of published values. Li & Leung (1987) further note that the light curve solution changes with epoch, and attribute this to variations in the degree of contact. However, it is more likely that changes in the light curve over timescales of a few years are due to variations in the placement, intensity, and/or physical extent of a hot spot, rather than physical changes in the system geometry.

Pavlovski et al. (1992) and Zola & Ogloza (2001) examine model light curves for V367 Cyg that include an accretion disk with a geometry that does not follow an equipotential surface for a static, non-rotating object. The models have difficulty matching the observations near secondary minimum, hinting at a light distribution in the disk that is more complicated than that adopted for the model. Wilson (1981; 2018) discusses models for systems that have large-scale accretion/decretion disks. Wilson (2018) generates a model light curve for a system with parameters like those expected for β Lyrae, and demonstrates that a large fraction of the variation in the light curve can be attributed to the disk. In the current paper it is shown that emission lines at visible wavelengths are strongest and also vary in strength with time near secondary minimum, which is the phase where the disk is eclipsed.

Zola & Ogloza (2001) conclude that the disk contributes $\sim 21\%$ of the system light in I , and estimate a mass transfer rate of $5 - 7 \sim 10^{-5} M_{\odot}/\text{year}$. This rate of mass transfer suggests that the mass ratio of the component stars will reverse on time scales of $< 10^5$ years if the lower mass estimates in Table 1 are correct. This timescale for mass reversal is roughly an order of magnitude faster than predicted for the systems modelled by Nelson & Eggleton (2001).

Another potential complication when modelling the V367 Cyg light curve is that there are other stars that contribute to the light. There is a companion that is ~ 5 magnitude fainter and 2.5 arcsec distant, and there are hints of another companion that is only ~ 0.15 arcsec (~ 300 AU) distant (e.g. Heiser 1961 and references therein, McAlister & Hattkopf 1988). Both of these objects fall within the plausible separation regime for physical companions (e.g. Simon 1997). Nelson & Eggleton (2001) suggest that companion stars and the resulting impact on angular momentum transfer are a possible explanation for the failure of their models to reproduce the properties of some Algol systems.

Light curve solutions have the potential to provide observational limits on the brightness of unresolved components via the inclusion of third light in the models (e.g. Davidge & Forbes 1988). This being said, Li & Leung (1987) find no evidence for third light in V367 Cyg light curves, while Zola & Ogloza (2001) find that models that include a disk provide only loose limits on third light. A close companion may explain at least some of the longer term photometric and spectroscopic variations that have been detected.

The examination of lines over a broad wavelength range from V367 Cyg is of interest to further explore the system properties. However, most spectroscopic studies of V367 Cyg have been at wavelengths shortward of $0.5\mu\text{m}$. In the present paper we discuss spectra of V367 Cyg that were recorded over seven months in 2021. The spectra span a $0.6\mu\text{m}$ wide wavelength interval centered on $\text{H}\alpha$ with a resolution $\frac{\lambda}{\Delta\lambda} \sim 17000$. With the exception of the spectra discussed by Tarasov & Berdyugin (1998) that cover only a few phase intervals and have narrow wavelength coverage centered on specific features, these wavelengths have not yet been examined in the spectrum of V367 Cyg.

2. OBSERVATIONS AND REDUCTION

The spectra were recorded with the 1.2 meter telescope and McKellar coudé spectrograph (Monin et al. 2014) at the Dominion Astrophysical Observatory (DAO). The detector was the 2048×4088 pixel SITe-4 CCD. This detector has $15\mu\text{m}$ square pixels and was binned perpendicular to the dispersion axis during read-out, with the level of binning set by other programs observed on a given night. The spectrograph was configured with the IS32R image slicer, the 32 inch camera, and the 1200H grating. The central wavelength was set near 6600\AA . This configuration produces a dispersion of $0.15 \text{\AA}/\text{pixel}$, with a resolution $\lambda/\Delta\lambda \sim 17000$.

The spectra were recorded with the telescope operating in robotic mode. Cloud cover was monitored with a wide-field camera, and the archived images indicate that some of the spectra were recorded during non-photometric conditions. The cloud cover on the non-photometric nights was such that the S/N ratio was not seriously compromised.

Three 300 sec exposures of V367 Cyg were recorded on each night, and the resulting 900 sec total exposure time produced a S/N ratio $\geq 100/\text{pixel}$ in the continuum. Heliocentric Julian Dates (HJD) on which spectra were recorded and the orbital phase at the time of observation are listed in Table 2. The spectra cover a full range of orbital phases, with the densest coverage near secondary minimum.

Phases were calculated using the ephemeris given by Lloyd (2018). The O–C diagram in Figure 5 of Lloyd (2018) shows a dispersion of one to two tenths of a day (~ 0.01 in orbital phase). This scatter may be due to transient events in the light curve, coupled with the comparatively long period of the system, which is such that eclipses occur over many hours, thereby complicating efforts to measure times of minimum on some nights.

A series of calibration frames were also recorded, and these were used to remove instrumental signatures from the spectra. The calibration suite includes biases, dispersed light

Date (HJD - 2459000)	Orbital Phase ^a	Date (HJD - 2459000)	Orbital Phase ^a
289.4589	0.45	417.2137	0.36
309.4723	0.56	419.4698	0.48
310.4730	0.62	420.4528	0.53
331.4905	0.75	421.2097	0.57
356.4316	0.09	422.2553	0.63
363.4322	0.46	437.1947	0.43
366.4206	0.62	438.3811	0.49
382.2732	0.48	439.2610	0.54
383.2663	0.53	440.2825	0.60
384.4197	0.59	441.2248	0.65
385.4529	0.65	444.2518	0.81
386.2690	0.69	445.1818	0.86
387.2709	0.74	446.4072	0.92
388.4228	0.81	468.1675	0.09
411.2179	0.03	470.2428	0.21
413.2834	0.14	471.1476	0.26
415.4502	0.26	481.1289	0.79
416.4374	0.31		

Table 2: Log of Observations

^aBased on the ephemeris calculated by Lloyd (2018).

from a continuum source to monitor flat-field variations, and spectra of a Th-Ar arc for wavelength calibration. The spectrophotometric standard star HR8634 (ζ Peg; Hamuy et al. 1992) was observed on some nights.

Processing was done with a standard pipeline for single slit spectra. The reduction sequence included bias subtraction, flat-fielding, wavelength calibration, and a correction to helio-centric velocities. The final step was the removal of variations in the continuum level to produce spectra with a pseudo-continuum normalized to unity.

3. THE RED SPECTRUM OF V367 CYG: AN OVERVIEW

The spectra were sorted according to orbital phase, and then binned in ten equally wide phase intervals. A mean spectrum was constructed for each bin to allow the properties of the spectra throughout a 'typical' orbital cycle in 2021 to be examined. These mean spectra are the subject of more detailed examination later in the paper. In this section, features are highlighted in the mean spectra at three phases to serve as an introduction to the more detailed analysis. This is done as the spectra cover wavelengths that have been little studied in V367 Cyg. Phase 0.5 (secondary minimum) is of particular interest given difficulties matching the light curve there (Pavlovski et al. 1992; Zola & Ogloza 2001).

The mean spectra at phases 0.3, 0.5 and 0.7 in three wavelength intervals are compared in Figures 1 – 3. The deep absorption lines in Figures 1 and 3 originate in the circumsystem shell. Variations in the shell lines that are related to orbital phase have been documented in past studies at shorter wavelengths (e.g. Heiser 1961; Aydin et al. 1978), and phase-related variations in line morphology are evident among the shell lines in our spectra. The SiII 6347 doublet is one of the strongest shell lines at these wavelengths. This is a resonance transition, and its behaviour with phase is not remarkable. Although not obvious in Figures 1 and 3, it is argued in Sections 4 and 5 that absorption lines from the donor star overlap with the shell lines, and that these contribute to the variations in the shell line profiles with orbital phase.

Broad emission features are evident in the shoulders of the FeII and SiII shell lines, and these vary with orbital phase. The emission lines associated with different FeII lines vary in sync and move in the opposite direction to that expected for an object associated with the donor star. FeII emission is most pronounced in the blueward shoulders of the shell lines near phase 0.5, when the accreting star and its disk is eclipsed. In Section 6 it is argued that these emission lines originate in the accretion disk.

There are other, less obvious, features in Figures 1 - 3 that are not related to the

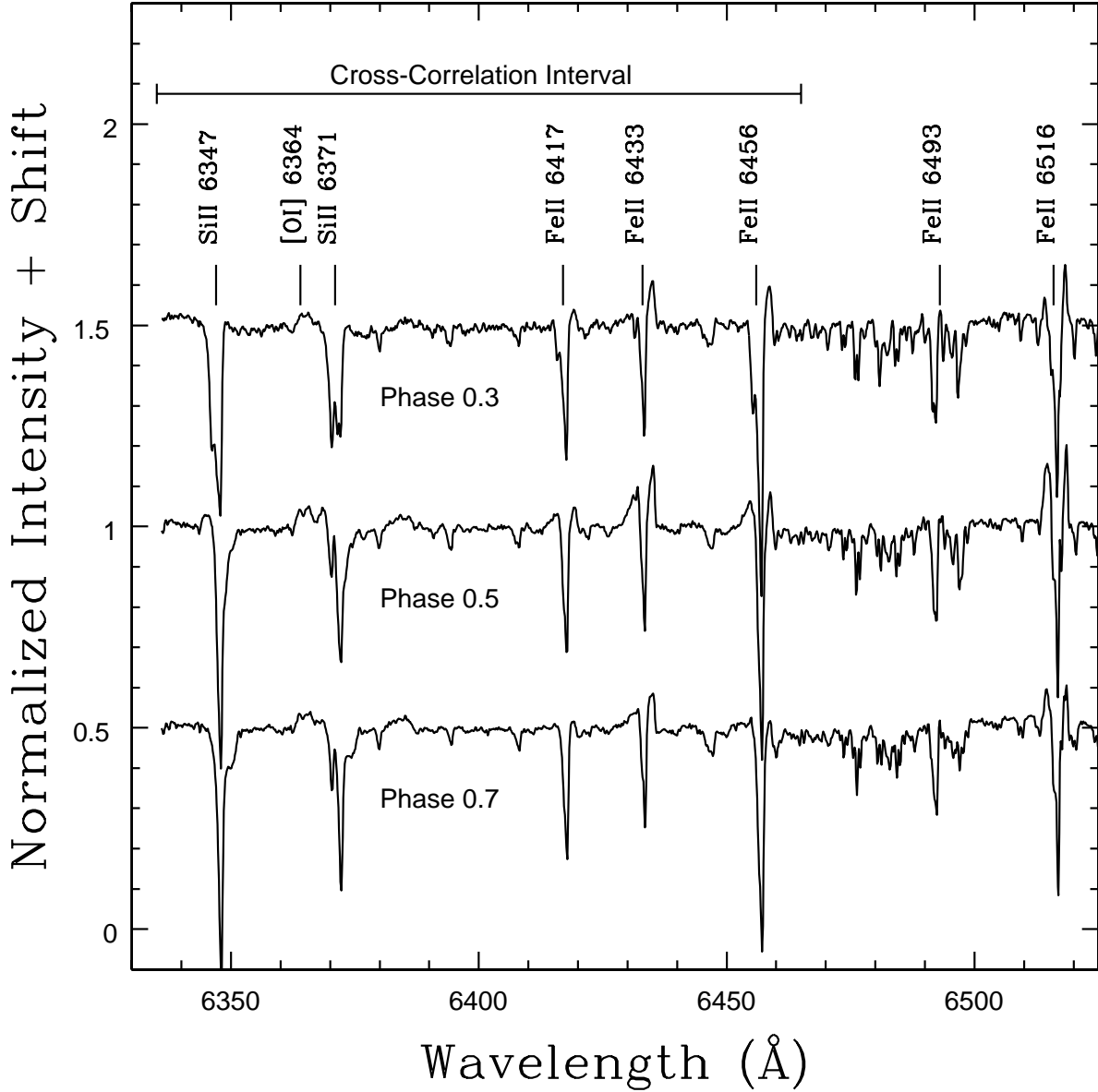


Fig. 1.— Binned spectra of V367 Cyg at three orbital phases in the wavelength interval 6330 – 6525Å . The spectra have been normalized to the continuum, and the results have been shifted vertically for display purposes. The main absorption components of the SiII and FeII lines originate in the circumsystem shell, and it is shown in Section 5 that there are transient absorption features in the shell lines that originate in the spectrum of the donor star. The emission features in the shoulders of the shell lines change with phase in a manner that is not consistent with a shell origin, and are strongest at phase 0.5, when the accreting star is eclipsed. [OI] 6364 is a broad, low amplitude emission feature, with a shape that varies with orbital phase. The wavelength interval used for the cross-correlation velocity measurements in Section 4 is indicated at the top of the figure.

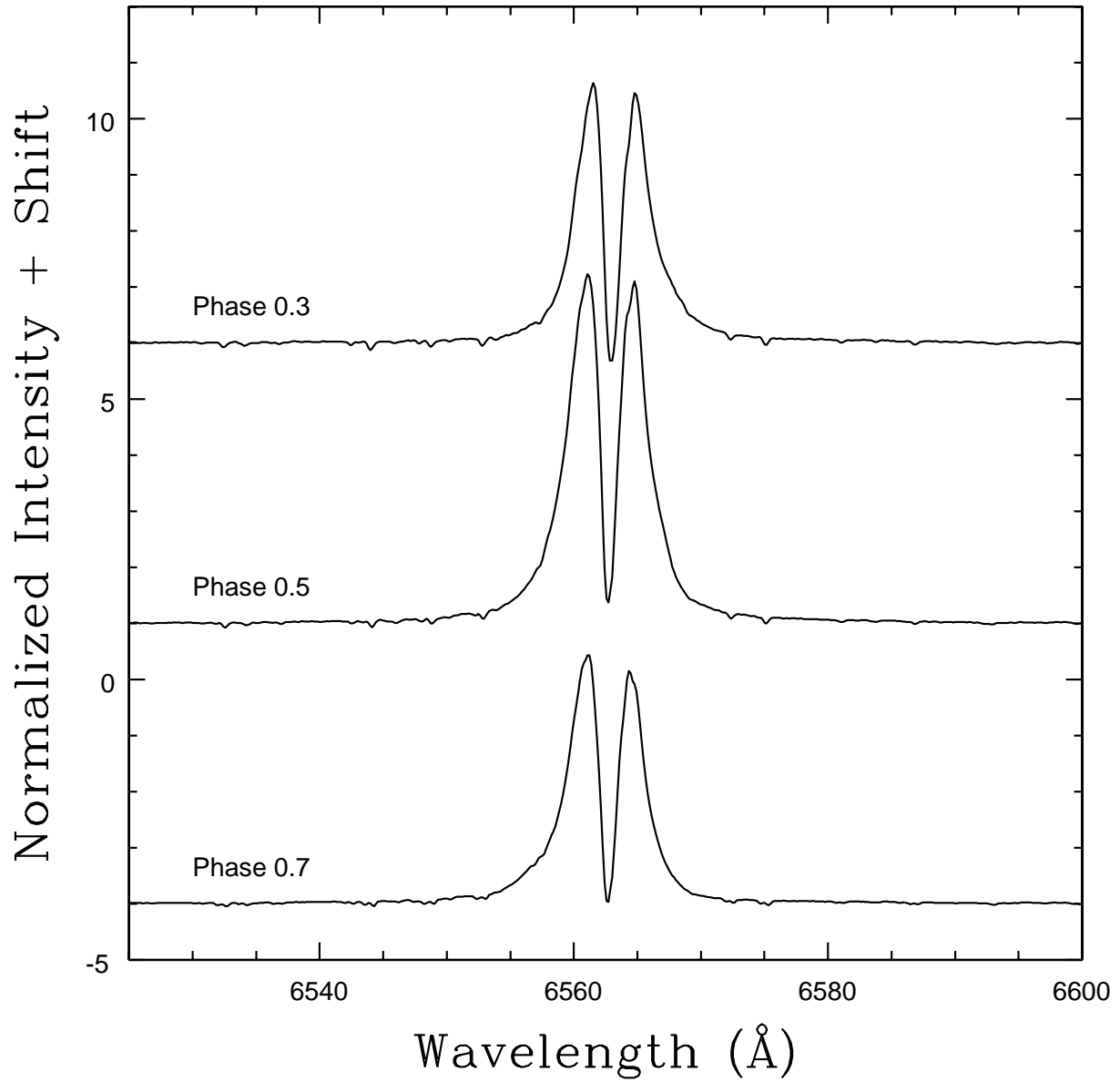


Fig. 2.— Same as Figure 1, but covering the wavelength interval 6525 – 6600 \AA . The dominant feature is H α , and the strengths of the emission and absorption components change with orbital phase. These components are most pronounced near primary minimum (not shown here) and secondary minimum.

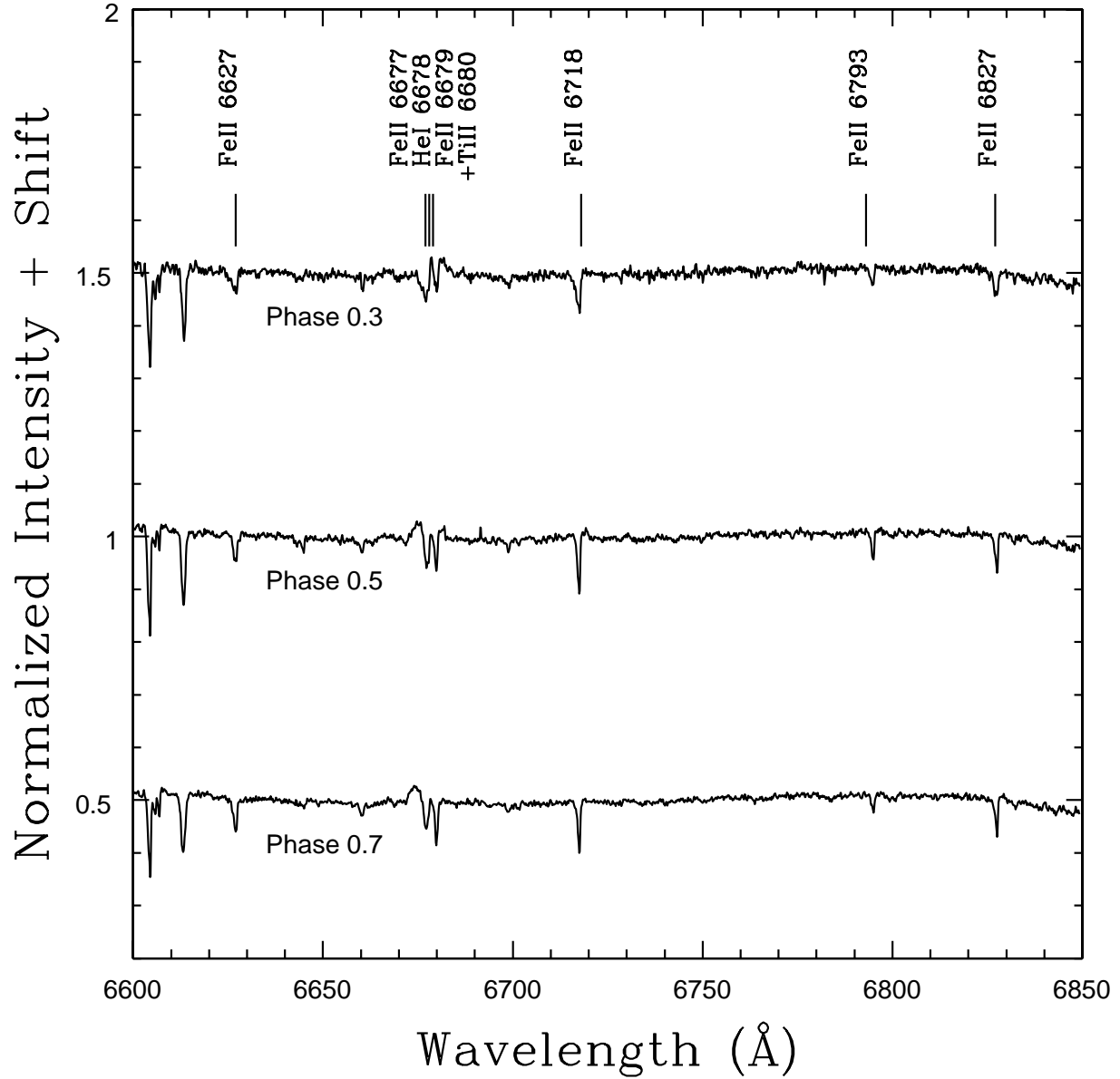


Fig. 3.— Same as Figure 1, but covering the wavelength interval 6600 – 6850 \AA . The shell lines at these wavelengths are weaker than those in Figure 1, but have similar transient features. HeI 6678 is located in a region that is dominated by shell absorption lines.

shell. The broad, low amplitude emission feature to the left of the SiII 6371 doublet in Figure 1 is [OI] 6364. The broad nature of this feature suggests that the emission forms in an environment that spans a range of velocities. In Section 6 it is shown that there is sub-structure that is related to orbital phase, and it is argued that there are two sources of [OI] 6364 emission. HeI 6678 in Figure 3 falls close to FeII and TiII shell lines that blend together at this wavelength resolution, and an obvious signature of HeI is not seen.

H α is the most conspicuous feature in the wavelength interval examined in this study, and absorption and emission components are evident in Figure 2. The character of H α changes with orbital phase in a manner that differs from that seen in the metallic lines discussed above. Phase-related variations in the characteristics of H α have been discussed by Tarasov & Berdyugin (1998), although with restricted phase coverage. The absorption and emission components in Figure 2 are most pronounced near phase 0.5; while not shown here, H α at phase 0.0 is similar in shape and strength to what is seen near phase 0.5 (Section 6). While higher order Balmer lines show characteristics that are suggestive of an origin in the donor star (e.g. Heiser 1961; Aydin et al. 1978), it is demonstrated in Section 6 that the donor star makes a negligible contribution to H α absorption.

4. THE SHELL SPECTRUM

4.1. The Shapes and Radial Velocities of Shell Lines

The morphologies of selected deep shell lines are examined in Figure 4, where phase-binned mean spectra of SiII 6347, SiII 6371, and FeII 6432 are shown. Phase-related sub-structuring is clearly evident in the line profiles, and this is most obvious in the SiII transitions. The most noticeable differences with orbital phase occur blueward of the line centers.

The SiII 6347 doublet is a resonance transition, and Tarasov & Bergyugin (1998) suggest that sub-structure in the SiII 6347 profile originates in a stream between the two stars. However, the variations in SiII 6347 with phase are mirrored in other Si and Fe lines - they are not restricted to SiII 6347. In Section 5 it is shown that a large part of the variations in the morphology of the shell lines are linked to the donor star and its radial velocity variation with orbital phase.

There is prominent emission in the redward shoulder of the FeII 6432 line, with weaker emission near the blue shoulder. The emission associated with FeII 6432 varies in wavelength with orbital phase, in the opposite sense to that expected for an object moving in sync with the donor star. The emission associated with this FeII line is broad and may not be centered on the absorption component. Moreover, it is not clear if the emission originates from a

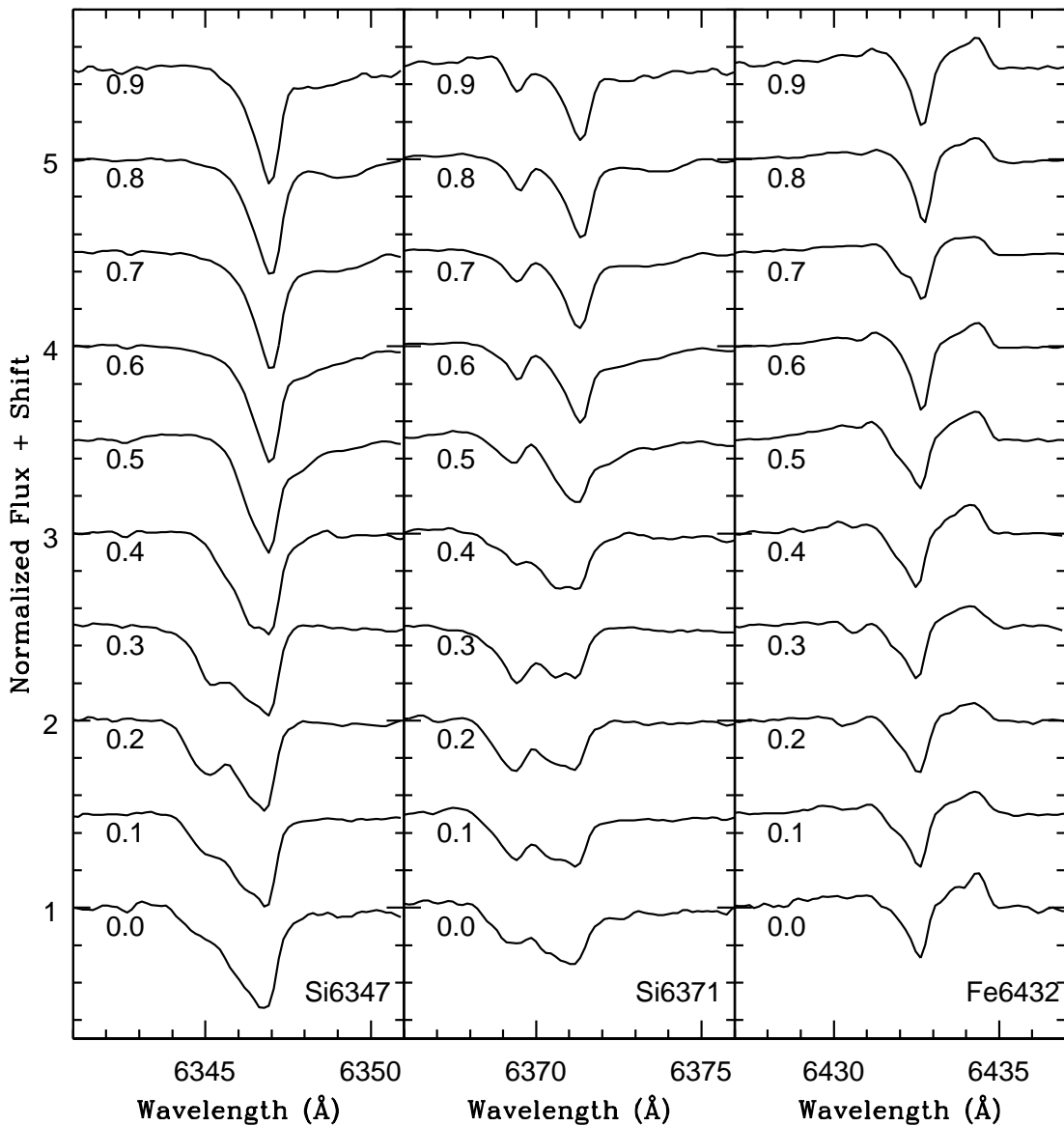


Fig. 4.— Mean phase-binned spectra centered on SiII 6347, SiII 6371, and FeII 6432. Orbital phases are listed near the left edge of each panel. Sub-structures propagate with phase through all three lines, and these are most evident at wavelengths blueward of the line centers. It is argued in this paper that much of this sub-structure is associated with the donor star. The emission associated with FeII 6432 is more pronounced than for the SiII lines, and it is argued that this emission originates in an accretion disk.

single source (i.e. there is no structure in the emission line), or if there are sub-components, such as is seen in [OI] 6364 (Section 6). Emission is also seen in the shoulders of the two SiII lines, although the relative strength of the SiII emission with respect to the depth of the absorption feature is lower than for FeII 6432.

Previous studies used line centroid measurements to extract velocities from the shell lines, and these concluded that the shell is rotating. However, it is not clear from Figure 4 if rotation is present. The red edge of the SiII and FeII absorption features remains more-or-less fixed in position with phase, although changes in the blue half of these lines might at first glance be interpreted as the result of velocity variations. Nevertheless, the variable nature of the shell line profiles raises the possibility that velocities obtained from line centroids may be skewed by changes in line structure with phase. Indeed, the sub-structures that are seen in Figure 4 indicate that line centroids that rely on the entire absorption component will not probe systematic shell velocities alone, but may instead be sensitive to transient line profile structures that may not originate in the shell.

Two sets of shell velocity measurements are discussed in the following sub-sections. Both sets of velocities were measured from phase-binned spectra that have been normalized to the continuum. The first set of radial velocities were measured via cross-correlation with a template spectrum in the wavelength interval $6335 - 6465\text{\AA}$. This wavelength interval, indicated in Figure 1, samples several deep shell lines, including the SiII 6347 resonance line. Cross-correlation techniques have the merit of yielding velocities in a consistent way that multiplexes the signal over a wide wavelength range. Of course, the resulting velocities are prone to biases introduced by transient features in line profiles given that the entire line contributes to the cross-correlation function. However, the peak of the correlation function is dominated by the deepest parts of the strongest lines, where contamination from transients is likely to be least important.

It is evident from Figure 4 that the deepest parts of shell lines are less susceptible to sub-structures than the shallower components. Therefore, a second set of velocities were obtained from the deepest parts of two Si and Fe lines. A comparison of velocities measured from Si and Fe lines provides a means of assessing if the emission component that is present in the shoulders of the Fe lines (e.g. Figure 4), but is weaker in the Si lines, skews shell velocity measurements.

4.1.1. *Cross-correlation velocities*

Cross-correlation velocities were measured in an iterative manner. An initial set of velocities were obtained using the Procyon spectral atlas spectrum (Griffin & Griffin 1979) as the template. The resulting cross-correlation functions have a clear peak from which velocities can be measured. However, the V367 Cyg spectrum is dominated by shell features, and not lines that form in a stellar photosphere. Therefore, the initial set of velocities were used to shift the mean phase-binned spectra into the rest frame. The alignment of features was checked, and a revised template for cross-correlation that is representative of the shell was then constructed by stacking the rest frame spectra and taking the median light level at each shifted pixel location. Taking the median signal at each pixel suppresses features that do not move in sync with the shell. In Section 4.2 it is shown that the median spectrum constructed in this manner faithfully tracks the shell absorption component at all orbital phases.

A refined set of velocities was then obtained by using the median spectrum as a template for the shell. It is not surprising that the use of the median shell spectrum as a template greatly increased the semblance of the correlation function. Differences of up to ~ 3 km/sec were found between the velocities obtained from the Procyon and shell templates, although the mean difference between the two sets of measurements is negligible, amounting to 0.1 ± 0.8 km/sec, where the quoted uncertainty is the 1σ standard error in the mean. The velocity curve obtained with the median shell template is shown in Figure 5.

The velocity curve obtained from the cross-correlation measurements is roughly sinusoidal with an amplitude of ~ 17 km/sec and $\pm 1 - 2$ km/sec jitter. Aydin et al. (1978) measured shell velocities from TiII, FeII, and CrII lines at blue wavelengths, and in Figure 5 the mean of these are compared with the cross-correlation velocities. The Aydin et al. (1978) velocities were extracted from the smooth curve shown in their Figure 4a. Aydin et al. (1978) state that their velocities were measured from ‘the deepest part of the lines, rather than midway between the wings’. The amplitude of velocity variations obtained from the cross-correlation measurements is much smaller than that defined by the Aydin et al. velocities.

4.1.2. *SiII 6347 and FeII 6432 velocities*

A second set of velocities were measured using the deepest parts of the SiII 6347 and FeII 6432 lines. These measurements were restricted to the bottom quarter of each line, as this is where the line profiles at most orbital phases are roughly symmetric, although the SiII

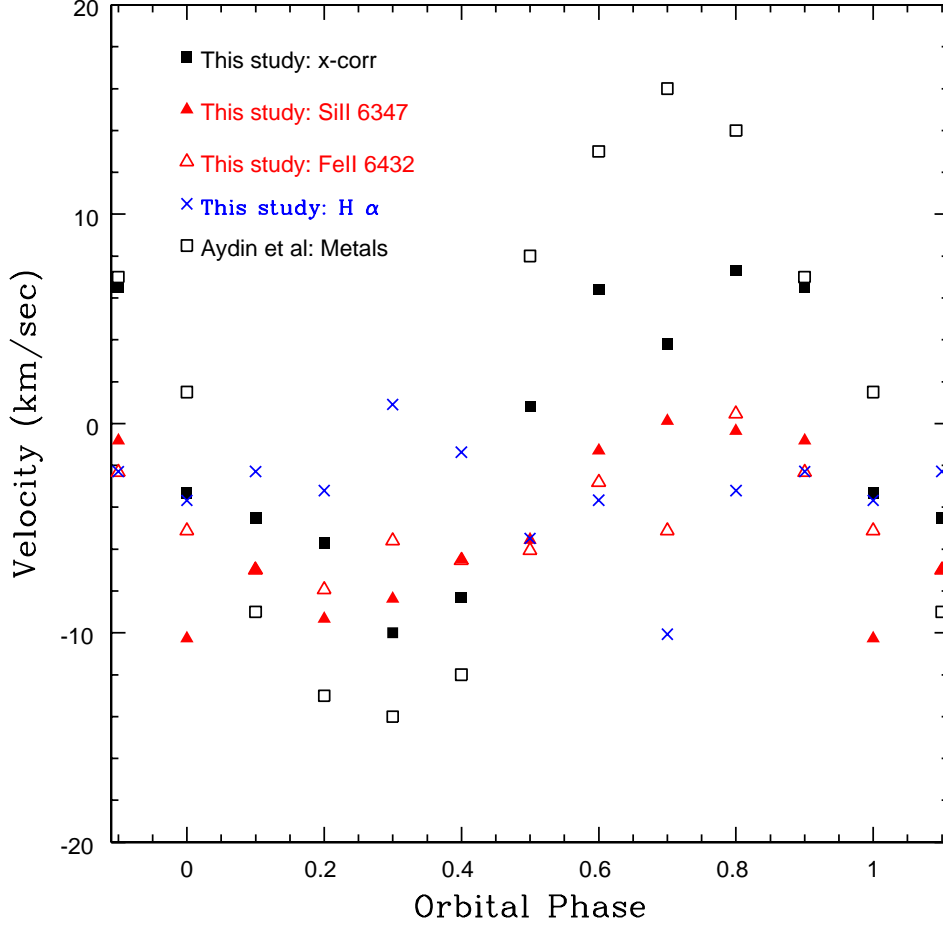


Fig. 5.— Velocities obtained from shell lines and $H\alpha$. The filled black squares are velocities measured in the wavelength interval 6335 to 6465Å using the iterative cross-correlation procedure that is described in the text. The open black squares are from the velocity curve based on metallic lines at blue wavelengths shown in Figure 4a of Aydin et al. (1978). The filled and open red triangles are velocities measured from the lower portions of the SiII 6347 (filled) and FeII 6432 (unfilled) absorption features, while the blue crosses indicate velocities measured in the deepest parts of $H\alpha$ absorption. The estimated uncertainty in our velocities is ± 1 km/sec. The velocity curves have different γ values, and this is attributed to contamination from the donor star spectrum in the upper half of the metallic shell absorption lines. The velocities obtained from SiII 6347 and FeII 6432 likely provide the most reliable estimate of the shell motion as they use the part of the line profile that is least affected by the donor star spectrum. Still, even those velocities may be skewed at some low level by sub-structure in the line profile. The $H\alpha$ velocities suggest motion in an opposite direction to that of the shell lines. The velocities used to construct this figure are tabulated in the Appendix.

line near phase 0.0 is a possible exception. Shell velocities measured from the deepest parts of these lines should then be less susceptible to distortions in the profiles than velocities determined from the entire line.

The velocities measured from the SiII and FeII lines are shown as red triangles in Figure 5. The velocity curves defined by these lines are more-or-less sinusoidal, with an amplitude of ~ 6 km/sec. This is considerably smaller than the amplitudes defined by the Aydin et al. (1978) and cross-correlation velocities shown in Figure 5. Moreover, with the exception of phase 0.0, where the SiII 6347 line in Figure 4 is distorted and the FeII 6432 is not, there is reasonable agreement between the velocities made from these two lines: once again, measurements made from the resonance SiII 6347 lines tend not to be exceptional. This agreement also suggests that the emission that is most pronounced in the shoulders of the FeII lines does not skew the velocity measurements.

4.1.3. Has shell rotation been detected?

We have presented evidence that distortions in the profiles of shell lines have likely biased shell velocity measurements in previous studies. Heiser (1961) reviews previous measurements that span a time baseline of many decades, and notes that the γ velocity of the shell velocity curve varies over timescales of a few years, spanning a ~ 30 km/sec range. However, the results in Figure 5 indicate that the γ velocity of the shell is susceptible to the procedure used to measure velocities. The γ value from the cross-correlation measurements is ~ 0 km/sec, while that obtained from the SiII and FeII measurements is ~ -4 km/sec. The Aydin et al. (1978) measurements in Figure 5 yield ~ 2 km/sec. We suspect that the variations in γ found in previous studies are due to differences in the method used to estimate the radial velocities of shell lines, rather than a physical shift in the mean shell velocity.

We suspect that the velocities made from SiII 6347 and FeII 6432 more faithfully track the true kinematics of the shell than the other measurements shown in Figure 5 as they are based on the parts of the profiles that appear to be least affected by distortions. Even then, the residual contamination evident in Figure 4 even near the line centers may still skew the results. Hence, the amplitude of the velocity measurements attributed to the shell may be even smaller than that found from these lines. A constant shell velocity with phase would be consistent with the azimuthal uniformity of the shell that is required to remove the shell component from the spectra at all orbital phases (Section 4.2).

4.2. Stability of the Shell Spectrum with Orbital Phase

Insights into the origins of the complex structure in the shell lines can be gleaned by examining the differences between individual mean phase-binned spectra and the median shell spectrum. Changes in the shape of the line profile with orbital phase could signal a non-uniform distribution of circumsystem material and/or contributions from sources that are not physically related to the shell. Differenced spectra, in the sense of the mean spectrum at a given phase minus the median shell spectrum at wavelengths centered on SiII 6347, SiII 6371 and FeII 6432 are shown in Figure 6. The median shell spectrum in each wavelength interval is also shown.

The differenced spectra in Figure 6 indicate that the dominant shell absorption feature at the rest wavelength of all three lines has been removed to within the few percent level at all orbital phases. Given that the phase-averaged spectra are constructed from observations that span a range of epochs, then the stability of each shell absorption line is consistent with a radially uniform distribution of material throughout the shell over many orbital cycles. This is consistent with hydrodynamical simulations of the mass outflow from model binaries that predict a shell that is smoothed by shocks at large radii (e.g. Bermudez-Bustamante et al. 2020).

While the main components of each shell line appear to have a stable depth over many orbital cycles, variations in the residual spectra with orbital phase are evident, and these are most pronounced in the SiII 6347 and SiII 6371 lines. Similar residuals are seen in the FeII 6432 line, although with a smaller depth than in the Si lines. The behaviour of the SiII 6347 resonance line is similar to that of the other metal lines, although in the next Section it is shown that small-scale sub-structures in the SiII 6347 lines may be present. The origin of the dominant feature in the residual spectra of each shell line is the subject of the next Section.

5. THE SPECTRUM OF THE DONOR STAR

Given that lines from the accreting star have not yet been detected, then only the spectrum of the donor star has been explored to date. Based on Mg II 4481 and other lines that may contain spectroscopic signatures of the donor star, Heiser (1961) assigned that star a spectral type A2, while Aydin et al. (1978) assign it type A5I-II. Estimates of the temperature of the donor star have ranged from 10000 K (Zola & Ogloza 2001) to 13450 K (Pavolvski et al. 1992). The rapid rotation of stars in CBSs complicates the relation between effective temperature and spectral-type (e.g. Yakut & Eggleton 2005). Large-scale

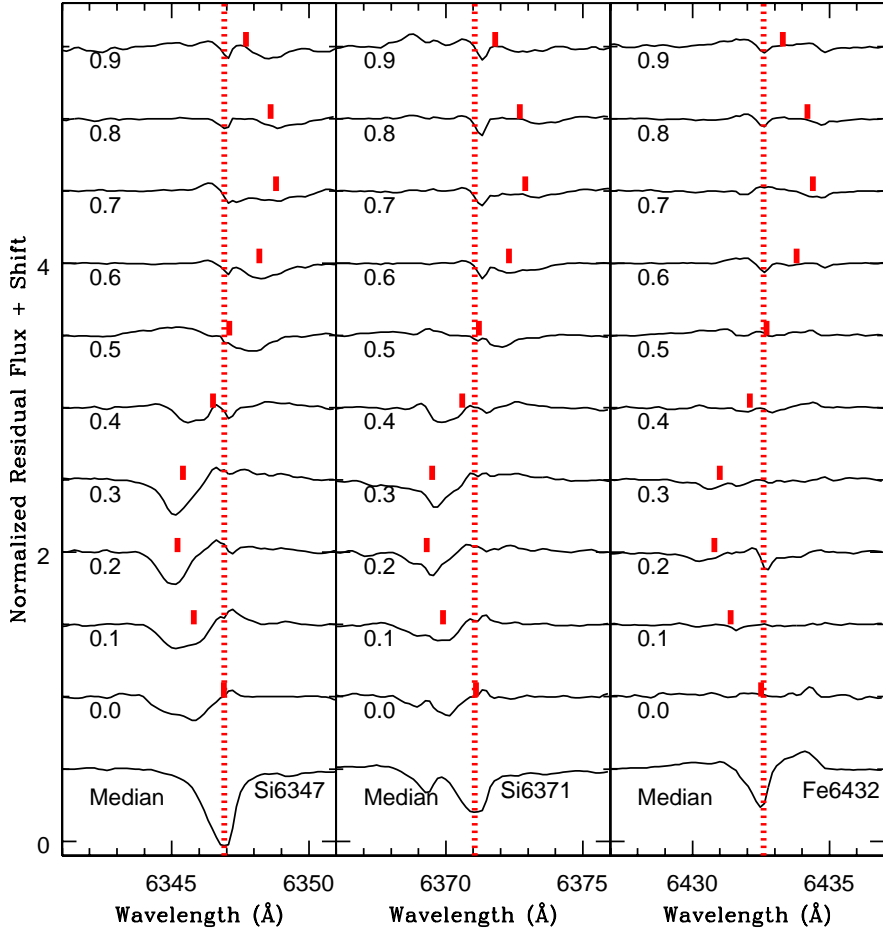


Fig. 6.— Differences between the median shell spectrum and the mean phase-binned spectra near SiII 6347, SiII 6371 and FeII 6432. The median shell spectrum is shown at the bottom of each panel. The dotted line marks the point of deepest absorption in each shell line, while the expected locations of the shell lines if they were in the spectrum of the donor star, assuming the composite velocity curve in Figure 6 of Tarasov & Bergyugin (1998), are indicated in red. There is a residual absorption feature that is deepest at phases 0.2 and 0.3 that follows a serpentine-like propagation with phase. The $\sim 3\text{\AA}$ throw of this feature in wavelength between the two quadrature points is consistent with that expected for the orbital motion of the donor star. SiII lines are among the deepest metallic signatures in the spectra of A-type stars at these wavelengths, whereas FeII lines tend to be weaker than the Si lines at those spectral types.

spot activity on the donor might also frustrate efforts to determine its spectral-type and effective temperature.

5.1. Extracting the Donor Star Spectrum

There is a compelling motivation to identify lines in the donor star spectrum over a range of wavelengths, as these can be used to examine basic characteristics such as the rate of rotation, chemical content, and effective temperature. Lines in the donor star spectrum have been identified at blue wavelengths (e.g. Heiser 1961; Aydin et al. 1978), and the most extensively studied of these is MgII 4481. An interesting finding is that spectra presented by Heiser (1961) and Aydin et al. (1978) show that the character of MgII 4481 changes with orbital phase, in the sense that it is deep and sharp near phase 0.25, but is weaker and broader near phase 0.75.

Lines in the donor star spectrum are detected in our data. There is prominent residual absorption in Figure 6 that weaves its way with wavelength through the SiII and FeII residuals. The change in the wavelength of these features from phase 0.2 to 0.6 is $\sim 3\text{\AA}$, corresponding to a ~ 140 km/sec velocity variation. This is consistent with the amplitude of the donor star radial velocity curve measured from MgII 4481 (e.g. Figure 6 of Tarsov & Berdyugin 1998). The vertical red lines in Figure 6 mark the expected location of the Si and Fe lines with orbital phase, working on the assumption that they originate in the photosphere of the donor star and that they follow the velocity curve of Tarasov & Berdyugin (1998). The absorption features in the residual spectra tend to have wavelengths that are consistent with an origin in the donor star spectrum. Moreover, the depths of the residual features in Figure 6 also vary with orbital phase, in a manner that is similar to that seen in MgII 4481.

Cycle-to-cycle changes in the mass transfer rate and/or the rate of mass deposition onto the accreting star could affect the outflow of material from the system, thereby producing structure in this material and signatures in shell absorption lines. Sub-structure in the mass flow might be most obvious in a resonance line, like SiII 6347, and the residual spectra of this feature do show subtle orbit-to-orbit variations. Evidence for this is shown in Figure 7, where residual spectra of SiII 6347 from the three epochs that are covered in the mean spectrum for phase bin 0.1 are shown. The spectra span a 4 month baseline, from May 2021 to September 2021.

There is prominent absorption centered near 6345\AA in the residuals, and the overall depth of this feature does not change markedly with time. The expected location of SiII

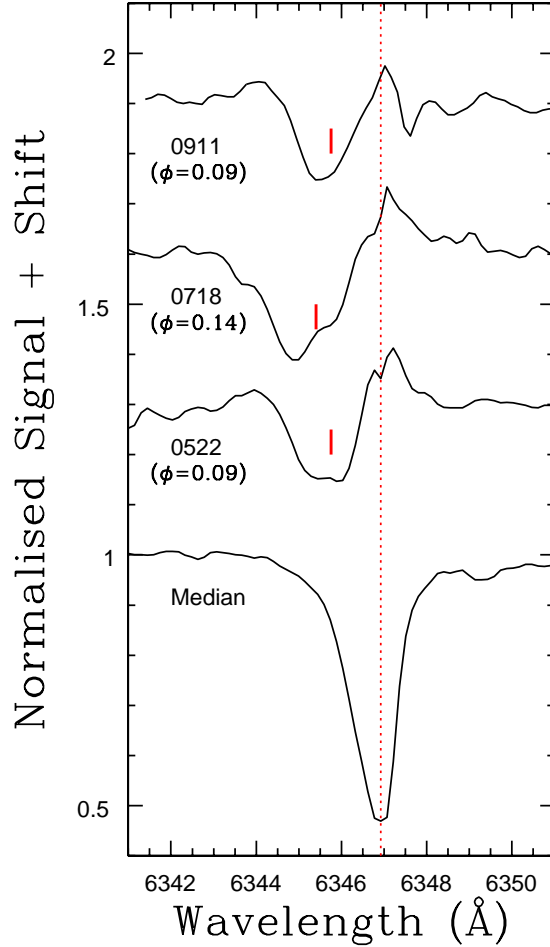


Fig. 7.— Residual structure in the SiII 6347 feature on three different nights that cover the phase interval 0.05 - 0.15. The orbital phase (ϕ) for each spectrum is shown. The residual spectra were constructed using the same procedure used to make Figure 6, and the dotted red line marks the wavelength where the shell line is deepest. The expected wavelength of SiII 6347 in the donor star spectrum at each orbital phase is indicated in red. The residual spectra on all three nights show broad absorption near 6345Å , and this is attributed to the donor star spectrum. There is evidence of a second feature near 6346Å that appears to weaken progressively with time over the range of dates sampled by the spectra. Thus, while much of the residual structure can be attributed to the donor star absorption spectrum, there may be transient components that originate in other sources.

6347 in the donor star spectrum if it were to follow the velocity curve shown in Figure 6 of Tarasov & Berdyugin (1998) is indicated by the solid vertical red line above each spectrum. The deepest feature in the residual spectra falls a few tenths of an Å blueward of the expected line position. This mis-match in the predicted and observed residual absorption feature is likely not due to an error in the velocity curve adopted for the donor star. It can be seen from Figure 6 that an offset between the expected and observed location of the residual absorption is restricted to the SiII 6347 line at phase 0.1, and increasing the overall amplitude of the velocity curve will result in a mis-match between the expected and observed line wavelengths at other phases. We thus suspect that not all of the sub-structure within the SiII 6347 line is associated with the spectrum of the donor star; while the central wavelengths of the residuals in Figure 6 tend to vary with orbital phase in a manner that is consistent with them tracking the motion of that star, signatures from other components might also be present.

A donor star spectrum can be constructed by shifting the phase-binned residual spectra to the rest frame after adopting a radial velocity curve for that star. The velocity-corrected spectra can then be combined to suppress artifacts in the residuals that are not due to the donor star. This basic procedure was adopted here, and donor star spectra were constructed for phases 0 - 0.5 and 0.5 - 1.0 given evidence that the depths of absorption features vary with phase.

The donor star spectra are shown in Figure 8, along with the mean spectrum that was constructed from all phases. Based on a model that assumes that the accreting star is enshrouded in a disk, Zola & Ogloza (2001) find that the donor star contributes 80% of the total system light at red wavelengths. Given the evidence of an accretion disk in the system, we adopt this fractional light contribution from the donor star. Therefore, the light levels of the donor star spectra in Figure 8 have been elevated by a factor of $1/0.8$ from their extracted values to display the strengths of features expected in the spectrum of a single star.

SiII and FeII absorption lines are seen in the donor star spectra. SiII 6347 and SiII 6371 are among the most prominent metallic lines in the spectra of A-type stars at these wavelengths, and the presence of these lines is perhaps not surprising given previous spectral-type estimates for the donor. In Section 5.2 it is shown that the depths of these lines are consistent with a mid-A spectral type.

The SiII and FeII lines are weaker and broader near orbital phase 0.75 than those near phase 0.25. The donor star spectra in the phase intervals centered on these phases also differ in the sense that there are emission components in the shoulders of the absorption lines that are shifted in different directions from the line centers. The nature of these shifts is consistent with the orbital motion of the accreting star. These are likely artifacts of emission

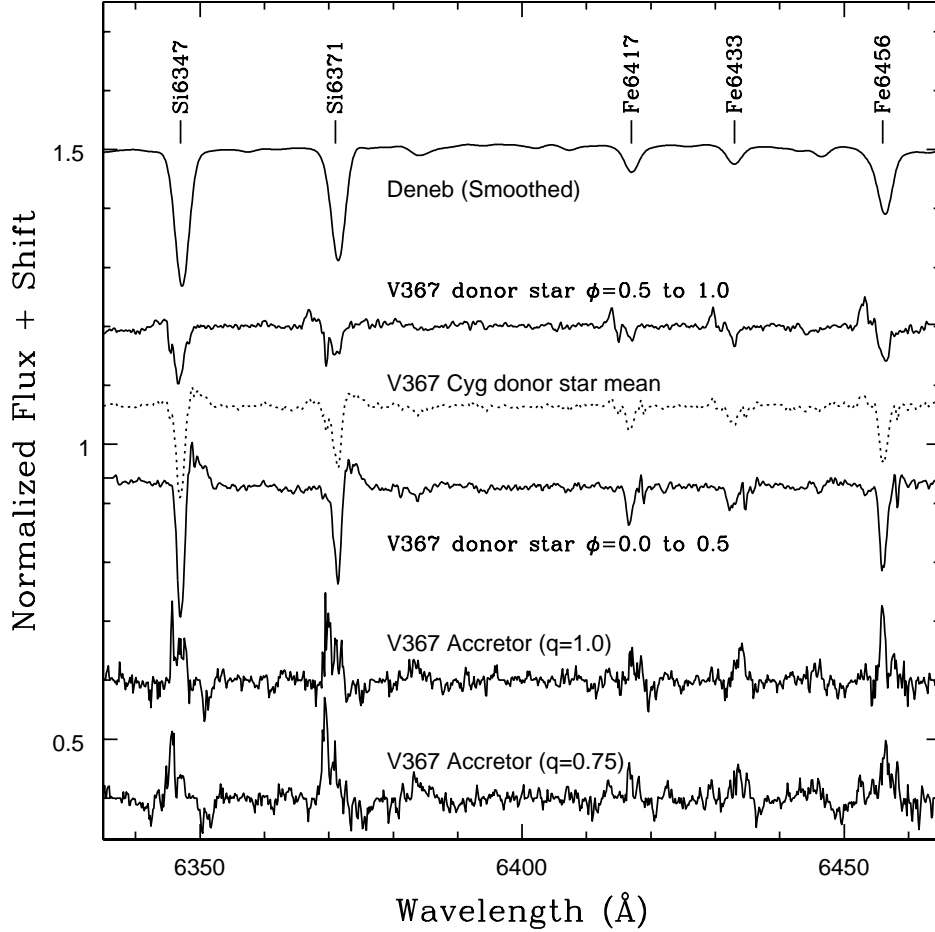


Fig. 8.— Spectra of – from top to bottom – Deneb, the donor star at different phases (ϕ), and the accretion disk. The Deneb spectrum has been smoothed to match the widths of lines in the mean donor spectrum. Donor star spectra in two phase intervals (0.0 to 0.5, and 0.5 to 1.0) are shown, as is the mean spectrum over all orbital phases (plotted as a dotted line). The spectrum of the donor star between phases 0.0 and 0.5 is similar to that of Deneb, suggesting that the donor star has features that are consistent with those of a mid-A giant/supergiant in this phase interval. The accretion disk spectra were constructed for two system mass ratios (q), and emission features of SiII and FeII are apparent. The strengths of the emission features are lower limits to their actual values given the procedure used to construct these spectra (see text). The donor star and accretor spectra have been scaled to produce lines with strengths that are appropriate for a single object, based on the relative luminosities listed in Table 2 of Zola and Ogloza (2001) in the R filter.

lines that originate in the accretion disk around that star, and these are seen throughout the residual spectra in Figure 6.

The variation in the depths of SiIII and FeII lines in the donor star spectrum with orbital phase is reminiscent of the behaviour of MgII 4481. Given that this similarity is based on Mg II spectra that were recorded at much earlier epochs, then the source of any phase dependency in the donor star spectrum has likely been stable for at least ~ 50 years, or almost 1000 orbital cycles. Such stability suggests that the donor star is tidally locked with the motion of the binary system at the present day, and this is consistent with the rotation velocity estimated from the line widths and some system geometries found from light curve modelling (see below). That the spectra differ at the quadrature points leads us to suspect that the phase-dependence of line strength is due to spot activity that covers much of a stellar hemisphere, such that it dominates the light over a wide range of orbital orientations.

The rotation velocity is an important parameter for stars in binary systems as rotation-induced mixing affects the internal structure of a star, and hence the pace of evolution and the properties of the final remnant (e.g. Taormina et al. 2020). If assumptions are made about tidal synchronization and geometric properties such as the Roche lobe fill factor then the rotational velocity can also be used to test system parameters. The widths of the SiII 6347 and SiII 6371 lines in the residual spectrum were measured in the donor star spectrum at phases 0.2 and 0.3, where these features are deepest and hence best defined. The line widths are consistent with $v \sin i \sim 54 \pm 2$ km/sec FWHM, where the uncertainty is the 1σ formal error in the mean. This is consistent with previous rotation velocity estimates for this star (e.g. Pavlovski et al. 1992). Moreover, this rotational velocity is consistent with a tidally locked donor star with a size of $21R_{\odot}$, as found by Zola & Ogloza (2001) from light curve models that include an accretion disk.

5.1.1. Comparisons with Deneb

Previous studies suggest that the donor star spectrum should be similar to that of an evolved A star, such as Deneb (spectral type A2Ia). Therefore, spectra of Deneb that were recorded as part of program DAO122-2015C4 (PI: Yang) were retrieved from the CADC archive and reduced using the same steps discussed in Section 2. These spectra were recorded with the DAO 1.2 meter telescope with the same instrumental configuration used to observe V367 Cyg.

The processed Deneb spectrum was smoothed with a Gaussian to match the widths

of the lines in the mean donor spectrum, and the result is shown in Figure 8. The SiII lines in the mean donor spectrum are weaker than those in the Deneb spectrum, although there is better agreement with the donor spectrum between orbital phases 0 and 0.5. Similar conclusions hold for the FeII lines. Between phases 0.5 and 1.0 the Si and Fe lines in the donor star spectrum are weaker than in Deneb. While the agreement with Deneb is not perfect, the comparisons in Figure 8 still indicate that the donor spectrum is consistent with that of an early to mid-A giant/supergiant. Extracting a donor spectrum at other wavelengths would help to better define the spectral-type of the donor.

6. EMISSION FEATURES

6.1. Si and Fe Emission Associated with the Accretor

V367 Cyg is a single line spectroscopic binary, and this frustrates efforts to obtain reliable component masses via traditional kinematic means. However, if lines from the accretion disk can be recovered then they can be used to trace the motion of the accreting star. Emission lines from accretion disks have been used to probe the orbital motions of white dwarfs in recurrent novae (e.g. Sahman et al. 2013). Tarasov & Berdyugin (1998) estimate stellar masses in V367 Cyg using a purported detection of HeI 6678 that they associate with the accretion disk.

The detection of spectroscopic signatures from the accretion disk is not an unreasonable expectation for V367 Cyg, as the light curve solution presented by Zola & Ogloza (2001), in which the secondary star is modelled as a disk, predicts that $\sim 20\%$ of the broad-band system light comes from that structure. The emission features in the shoulders of the absorption lines propagate in the opposite direction to features that originate in the donor star spectrum (e.g. Figure 6), leading us to suspect that they form in the disk around the accreting star.

A complicating factor when attempting to reconstruct the emission line spectrum is that the central regions of these lines are obscured by shell absorption. Still, if a system mass ratio is assumed then residual spectra at various phases can be placed into the rest frame of the accreting star, and the results combined to search for spectroscopic signatures associated with that star and/or the surrounding disk. While this will likely yield spectra with compromised line strengths due to shell absorption lines, it may still provide clues into the nature of the emission – for example, are there spectroscopic similarities with other early-type stars that have accretion disks?

The results of combining the residual spectra if system mass ratios of unity and 0.75 are assumed are shown at the bottom of Figure 8. These spectra were constructed by taking

the median signal at each aligned pixel after shifting to the rest frame using velocities for the accreting star calculated from the Tarasov & Berdyugin (1998) radial velocity curve for the donor star. The spectra have been scaled upwards using the R-band luminosity for the disk listed in Table 2 of Zola & Ogloza (2001). A spectrum was also constructed for a mass ratio of 0.5, and the emission features in that spectrum are much weaker than in the spectra that assume higher mass ratios. This suggests that the system mass ratio is > 0.5 .

The spectra for mass ratios of 0.75 and 1 are very similar. Given the presence of prominent emission features in the observed spectra that move in sync with the expected motion of the accreting star then it is not surprising that line emission is present in the combined spectra. However, the accretion spectra in Figure 8 are noisy, and this is contrary to what might be expected given the prominent emission lines in the unphased spectra. We emphasize that the strengths of the emission lines in Figure 8 are lower limits to their actual values because the central regions of the emission lines overlap with the shell absorption lines, with the result that much of the signal in the central part of the emission line is lost when constructing the residual spectra. This produces the clipped appearance of the emission lines in Figure 8. The absorption features from the donor star are also broadened by rotation, and at least some level of coherence in the donor star spectrum is retained. This will also affect the strengths and widths of accretion disk features.

An examination of the excitation mechanisms that power the emission is frustrated by the problems recovering reliable line strengths and widths. Still, we note that Fe and Si emission lines are seen in the spectra of other types of objects in which early-type stars are surrounded by an accretion disk, including Herbig AeBe stars (e.g. Hernandez et al. 2004) and classical Be stars (e.g. Mathew & Subramaniam 2011). This similarity extends to other features in the V367 Cyg spectra, such as $H\alpha$ and [OI] 6364, and these similarities are discussed in the following sections.

6.2. $H\alpha$

Tarasov & Berdyugin (1998) discuss the behaviour of $H\alpha$ in V367 Cyg, and find that there is prominent emission with deep central absorption. The characteristics of both the emission and absorption components were found to remain constant with orbital phase, although the Tarasov & Berdyugin spectra have limited phase coverage, with three of their four profiles covering orbital phases between 0.6 and 0.8. The spectra recorded for this study track $H\alpha$ over a full range of phases.

Mean phase-binned spectra centered on $H\alpha$ are shown in the left hand panel of Figure

9. Previous studies have identified absorption from higher order Balmer lines that is believed to originate in the donor spectrum. The spectrum of the A-type supergiant Deneb is shown in Figure 9. To the extent that Deneb is a good match to the spectrum of the donor star then it is clear that the donor makes only a modest contribution to the observed $H\alpha$ absorption.

When interpreted in the scheme described by Reipurth et al. (1996) for Herbig AeBe stars, the $H\alpha$ profiles would be classified as Type II, which are the most common type of profile (e.g. Viera et al. 2003). $H\alpha$ emission in V367 Cyg is likely circumsystem in origin, forming in material that has been ejected from the system. This is consistent with the modest shifts in wavelength with orbital phase that are evident in Figure 9.

6.2.1. $H\alpha$ variations with phase

There appears to be a slight change in the central wavelength of $H\alpha$ with orbital phase, suggesting a variation in radial velocity. This being said, the asymmetric nature of the $H\alpha$ absorption profile is a source of uncertainty when measuring velocities. As these asymmetries appear to be smallest near the bottom of the $H\alpha$ absorption line then we have measured velocities from that part of the profile, and the results are compared with the donor star and shell velocities in Figure 5.

The amplitude of the velocity variation defined by $H\alpha$ is small, and a systematic variation with phase is not seen. Still, the velocities near phases 0.25 and 0.75 hint at an orbital motion in the same direction as the accreting star. Tarasov & Berdyugin (1998) find evidence of a 15 km/sec systematic shift in the velocity of $H\alpha$ when compared with other features. Three of their four profiles are between phases 0.6 and 0.8, and this is where the largest departure from the mean $H\alpha$ velocity is seen in our measurements.

The shapes and central wavelengths of the $H\alpha$ absorption and emission components in Figure 9 change with orbital phase. To examine these changes, the spectra were aligned using the velocities measured from $H\alpha$ absorption discussed above, and a mean spectrum was generated. The mean spectrum was then subtracted from each of the phased-binned spectra, after they too had been aligned using the velocity measurements made from $H\alpha$ absorption. The residual spectra are shown in the right hand panel of Figure 9.

$H\alpha$ changes with orbital phase. The largest deviations from the mean spectrum occur at the eclipses, in the sense that the absorption and emission components have the largest residuals at these phases. This helps to explain why variations with phase were not detected by Tarasov & Berdyugin (1998), as none of their spectra fell within ± 0.05 in phase of an eclipse. The variation in $H\alpha$ strength with phase in Figure 9 could be a geometric effect in

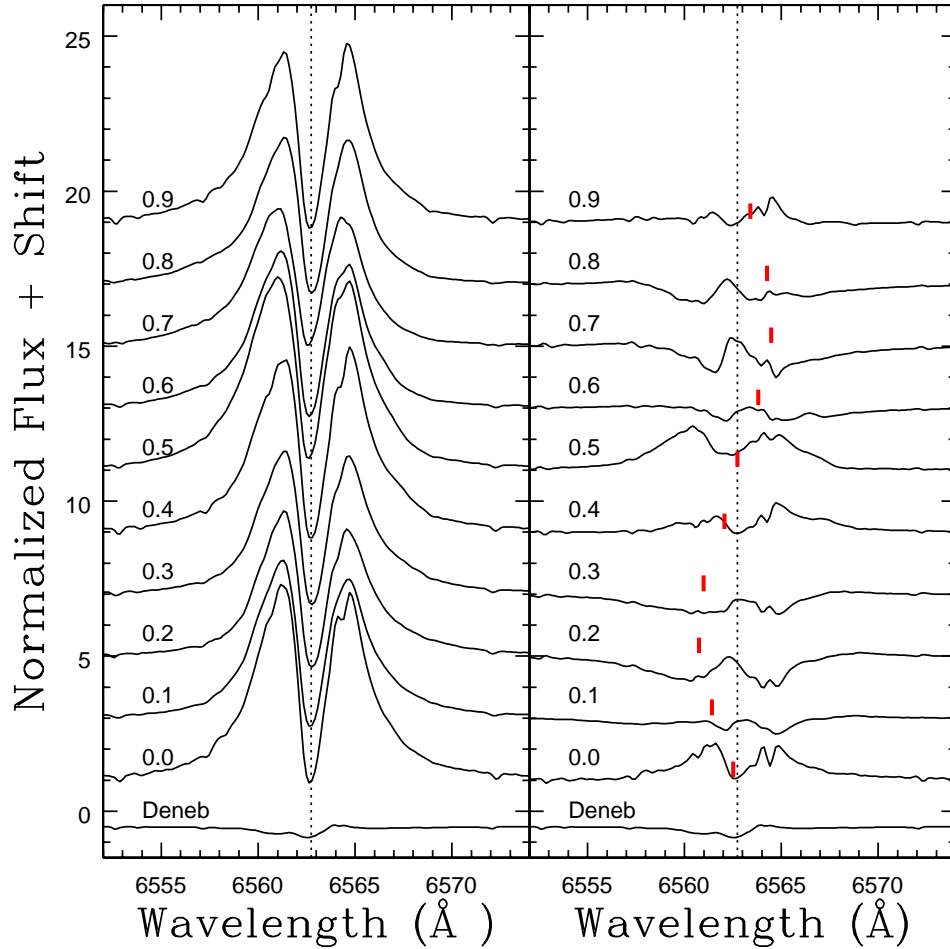


Fig. 9.— Left hand panel: Phase-binned spectra centered on $H\alpha$. The spectrum of Deneb is shown at the bottom of the panel, and it is evident that $H\alpha$ absorption from an A supergiant spectrum like that of Deneb makes only a modest contribution to the total $H\alpha$ absorption. The dotted line indicates the mean midpoint of $H\alpha$ absorption, as measured from the lower portions of the line profiles. Modest changes in the central wavelength of the absorption component and in the shape of the emission component are apparent. Right hand panel: Differences between the composite mean $H\alpha$ spectrum constructed by averaging the spectra at all ten phases and the phase-binned spectra. The residuals highlight changes in the amplitude of the emission and absorption features with orbital phase. The expected location of $H\alpha$ absorption in the donor spectrum is indicated with red lines, and any signatures of this feature are swamped by noise in the residuals.

which the binary system blocks light from some of the emitting gas outside of eclipse.

We have examined if signatures of $H\alpha$ absorption from the donor star spectrum can be seen in the residual spectra. The expected wavelengths of $H\alpha$ absorption in the donor star spectrum at various phases are marked in the right hand column of Figure 9. These wavelengths were calculated using the Tarasov & Berdyugin (1998) composite velocity curve for the donor star. Absorption features are not seen at the expected wavelengths. That $H\alpha$ absorption from the spectrum of the donor star has not been detected is likely due to the broad and strong $H\alpha$ emission component that is present at all orbital phases, coupled with noise in the residuals.

6.2.2. $H\alpha$ near secondary minimum

$H\alpha$ emission and absorption are stronger than average near secondary minimum, and this is also where there are difficulties matching the light curves (e.g. Zola & Orgloza 2001). As the dominant feature in the red spectrum, the behaviour of $H\alpha$ at phases near secondary minimum may provide clues into the origin and distribution of light in that part of the light curve. This motivated us to examine individual spectra that were recorded on individual nights and that sample the 0.45 - 0.55 phase interval.

There are eight spectra in our dataset that sample phases between 0.45 and 0.55, and residual $H\alpha$ spectra for these nights are shown in Figure 10. The residuals are the result of subtracting the mean spectrum constructed from all orbital phases from each spectrum. The results are ordered according to the offset in phase from secondary minimum, such that those closest to secondary minimum are shown at the top, and phases that are progressively more removed from secondary minimum are placed towards the bottom of the figure. This display scheme allows the symmetry of $H\alpha$ about secondary minimum to be evaluated, while also enabling a search for variations with time.

There are obvious differences between the spectra at phases 0.46 and 0.54, in the sense that $H\alpha$ is weaker at phase 0.54. We suspect that this difference is likely due to variations in the strength of $H\alpha$ over timescales of a few months, rather than due to orbital phase. More specifically, there are significant differences between spectra that sample the same phase but that were recorded on different dates. These differences are such that $H\alpha$ emission from the system appeared to be stronger during March - June 2021 than during July - August of that year. The two spectra at phase 0.48 are separated in time by only 37 days, indicating that the $H\alpha$ strength varied considerably over only two orbital cycles. When considered in the context of an outflow model, such as that discussed by Deschamps et al. (2015), the

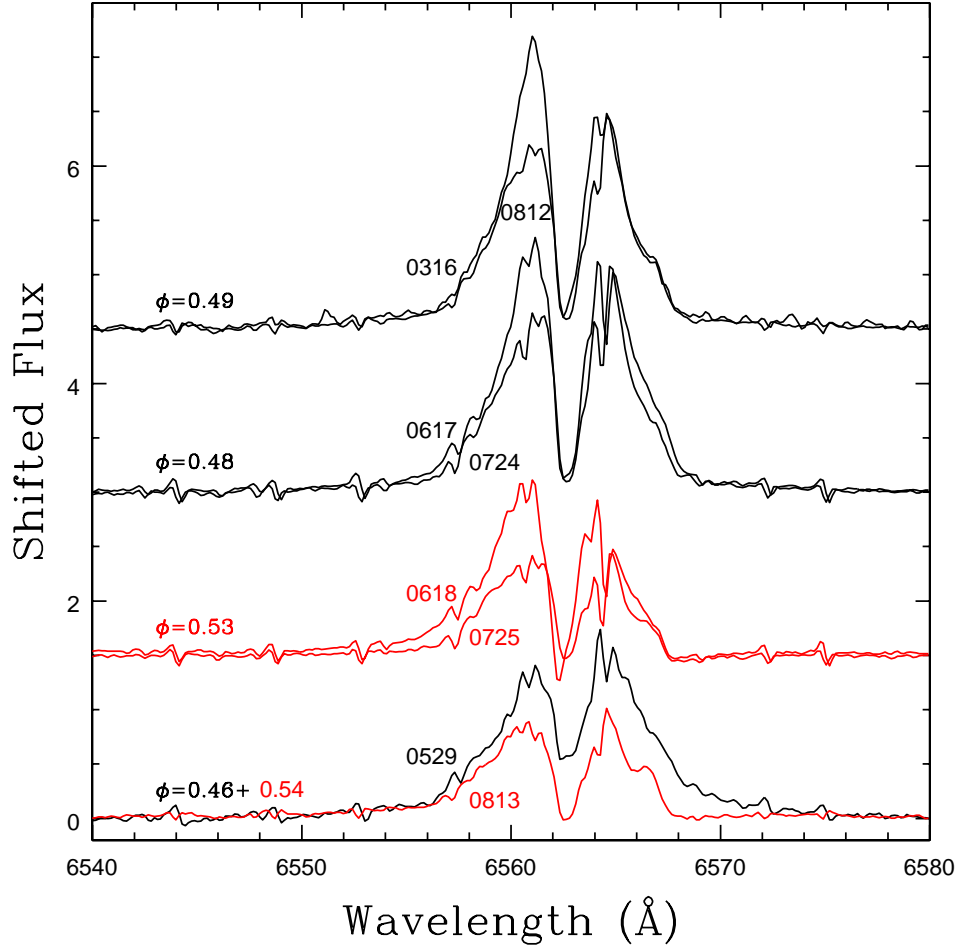


Fig. 10.— $H\alpha$ residuals near secondary minimum (phase 0.5). Each curve shows the result of subtracting the phase-averaged mean spectrum from an individual spectrum. Spectra are grouped using orbital phase bins having a width of 0.01 phase units, and the spectra are identified by the month and day in that month (e.g. March 16 = 0316). The residual spectra are displayed folded about phase 0.5 so that the brightening and fading of $H\alpha$ can be compared before and after secondary minimum. The spectra at the top are closest to secondary minimum in terms of orbital phase, while the spectra at the bottom are furthest from secondary minimum. Spectra recorded with phases between 0.51 and 0.55 are shown in red. There are differences between the spectra at each phase offset from secondary minimum, and it is argued in the text that these are likely due to variations in $H\alpha$ strength with time, rather than orbital phase, in the sense that $H\alpha$ emission was consistently stronger during March – June 2021. There is also evidence for systematically stronger $H\alpha$ emission towards phase 0.5, based on the strengths of spectra that were recorded only one day apart in June (0617 and 0618) and July (0724 and 0725).

variations in the strength of $H\alpha$ emission with time that are seen in Figure 10 could be due to enhanced ejection rates and clumpy structure in the outflow, as might form if material is not ejected from the system at a uniform rate.

In addition to evidence that $H\alpha$ varies with time, the residual spectra in Figure 10 indicate that $H\alpha$ varies in a systematic way with orbital phase. There are two sets of spectra recorded in June and July that are separated by only 1 day (~ 0.05 in orbital phase), and these show a clear tendency for $H\alpha$ to be stronger at phases closest to secondary minimum. Both time and orbital phase thus appear to affect the strength of $H\alpha$ emission near secondary minimum. As the $H\alpha$ flux during ingress and egress of secondary minimum appears to be symmetric with phase, then the variation of $H\alpha$ with time may have contributed to difficulties matching secondary minimum in the light curves.

6.3. [OI] Emission

Broad [OI] emission with a width of $\sim 4.5 \text{ \AA}$ is present at all phases. [OI] 6364 will be accompanied by the much stronger [OI] line at 6300 \AA , although this transition falls just outside of the wavelength range covered by our spectra. Herbig AeBe stars may provide some insights into the origin of [OI] emission in V367 Cyg. [OI] 6364 is seen in the spectra of many Herbig AeBe objects (e.g. Bohm & Catala 1994), where there is evidence that it is associated with an optically thick disk and outflow (e.g. Corcoran & Ray 1997, Viera et al. 2003, Acke et al. 2005). [OI] 6364 emission in these stars is often accompanied by Si and Fe emission lines, such as are seen in the shoulders of the shell absorption lines that have been the focus of much of this paper. [SII] 6716 and 6731 emission can also be present. Figure 3 shows hints that [SII] 6731 might be present at some phases, although it is very weak. Efforts to detect [SII] 6716 emission in Figure 3 are frustrated by the FeII 6718 shell line.

While the spectra of most Herbig AeBe stars have a pronounced [OI] emission peak (Bohm & Catala 1994), this is not the case here. Rather, the broad nature of [OI] 6364 in the V367 Cyg spectrum suggests that it originates in an environment with a $\pm 100 \text{ km/sec}$ velocity dispersion. The shape of the [OI] 6364 profile also changes with orbital phase. This is demonstrated in Figure 11, where phase-binned spectra are shown in the left hand panel. The results of subtracting the phase-averaged spectrum are shown in the right hand panel of this figure. Contamination from SiII 6371 emission blueward of the main shell absorption lines can be seen near 6367.5 \AA in the spectra at phases 0.0 and 0.1 (see also Figure 1).

It has been suggested that [OI] emission from Herbig AeBe stars originates in a circumstellar disk that is undergoing Keplerian rotation (e.g. Acke et al. 2005). The structure

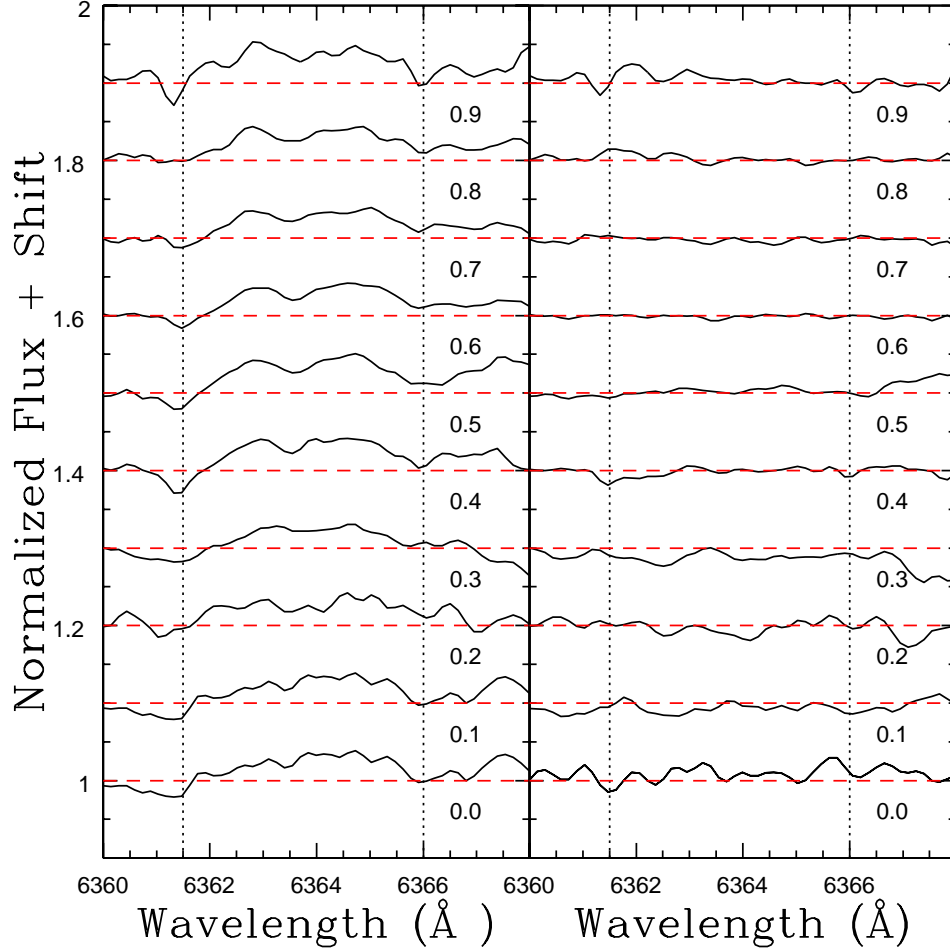


Fig. 11.— Left hand panel: Mean phase-binned spectra of [OI] 6364. The continuum level for each spectrum is indicated with a red dashed line, while the dotted lines mark the approximate blue and red boundaries of the emission. Emission in the blue part of the [OI] feature is weakest at phases 0.0 and 0.1. The component in the blueward part of the line grows in strength towards progressively later orbital phases, while the strength of the redward signal stays roughly constant. Right hand panel: Differences between a composite mean spectrum constructed by averaging the spectra at all ten phases and individual phase-binned spectra.

that is seen in the [OI] 6364 emission suggests that there may be multiple emission sources, although there is evidence that a sizeable fraction of this emission may come from the accretion disk. In particular, there is a tendency for the emission at the short wavelength portion of the feature to strengthen towards later phases, while the emission at redder wavelengths stays more-or-less constant. This is reminiscent of the behaviour of the SiII and FeII emission components seen in the shoulders of the shell lines. We have not attempted to measure velocities from [OI] 6364 given that this is a broad, complex feature. However, we note that [OI] emission in Figure 11 spans the wavelength range that would be expected if the feature originated in a disk that moved with the secondary star if the system had a mass ratio near unity.

Blue-shifted [OI] 6300 emission is a common feature in Herbig AeBe stars. The most extreme cases are associated with stellar jets and outflows in which light from corresponding red-shifted emission is blocked by the disk (e.g. Corcoran & Ray 1997, Acke et al. 2005). A component of the [OI] emission from V367 Cyg might also originate in an outflow, that presumably originates from the hot spot or the outer Lagrangian points. If present, then such a component would likely contribute to the red side of the [OI] emission, as that part of the line appears to be stable with phase. An examination of [OI] 6300 will provide additional insights into the origins of [OI] emission from V367 Cyg.

6.4. HeI 6678

Given that they are experiencing rapid mass transfer, W Ser systems are expected to contain a hot spot where the mass stream strikes the accretion disk. If it has a high enough effective temperature then this hot spot has the potential to power some of the unusual spectroscopic features associated with these systems, and also explain some of their unusual photometric properties, including features in the light curve that are not attributed to the component stars. Table 1 of van Rensbergen et al. (2011) provides a compilation of hot spot temperatures on the accretion disks of W Ser systems, and in many cases the temperatures are high enough to power HeI emission. While not expected to originate directly from the photospheres of the stars in V367 Cyg, a search for HeI 6678 emission is then warranted.

Tarasov & Berdyugin (1998) discuss efforts to detect HeI 6678 emission from V367 Cyg. They identify a feature with radial velocities that are consistent with those expected for the accreting star and its accompanying accretion disk, and identify it as HeI 6678. However, HeI 6678 is at a wavelength where there are also shell absorption lines (e.g. Figure 3), and this lead Zola & Ogloza (2001) to question the HeI detection. In addition to the obvious problems caused by the crowding of features in the spectrum, the metallic shell lines have

absorption and emission components, and the wavelength of the emission varies with orbital phase in a manner that is consistent with the motion of the accreting star (e.g. Figure 3). The emission from these metals might then be misinterpreted as originating from another element with a similar wavelength, such as HeI.

Mean phase-binned spectra at wavelengths near HeI 6678 are shown in the left hand column of Figure 12, and the median of these is shown at the bottom of the panel. Shell lines bracket the expected location of HeI 6678. The right hand portion of Figure 12 shows the results of subtracting the median spectrum from each phase-binned spectrum, and there are subtle changes at wavelengths near the two shell lines with orbital phase that are likely due to the orbital motion of the donor star (Section 4).

The vertical red lines in the right hand panel of Figure 12 mark the expected location of HeI at each phase if it followed the velocity curve measured by Tarasov & Berdyugin (1998). An emission line near 6679Å is seen in the residual spectra at phase 0.0 (i.e. primary minimum), and this falls within the wavelength range expected for HeI in this phase bin. This line is also visible in the left hand panel, indicating that it is not an artifact of the removal of the median spectrum, but a real detection. We thus consider this to be a tentative detection of HeI 6678 at an orbital phase when the accreting star and its accompanying disk eclipse the donor star. The confirmation of this detection could be examined further with additional spectra of V367 Cyg, although with the caveat that if the hot spot moves on the accretion disk then the HeI line will appear at another phase.

While our spectra hint that HeI 6678 is visible near primary minimum, it is not detected over a full orbital cycle. To demonstrate this, median spectra were constructed by aligning and combining the residual spectra according to the Tarasov & Berdyugin velocities (i.e. a mass ratio of 0.5) as well as for a mass ratio of 0.75, and the results are shown at the bottom of the left hand panel. The combined spectra are featureless, with no feature near the expected HeI wavelength. We conclude that while there is possible evidence for HeI 6678 near primary minimum, it is not detected throughout the orbital cycle of the system. This is consistent with the HeI 6678 emission being powered by a source such as a hot spot that is not visible at all orbital phases.

7. IR EMISSION AROUND V367 CYGNI

Mass transfer in a CBS may not be a conservative process. The loss of mass and angular momentum from the system hinders efforts to deduce the properties of the progenitor stars in present day Algol systems (e.g. Nelson & Eggleton 2001), and to predict the final evolution

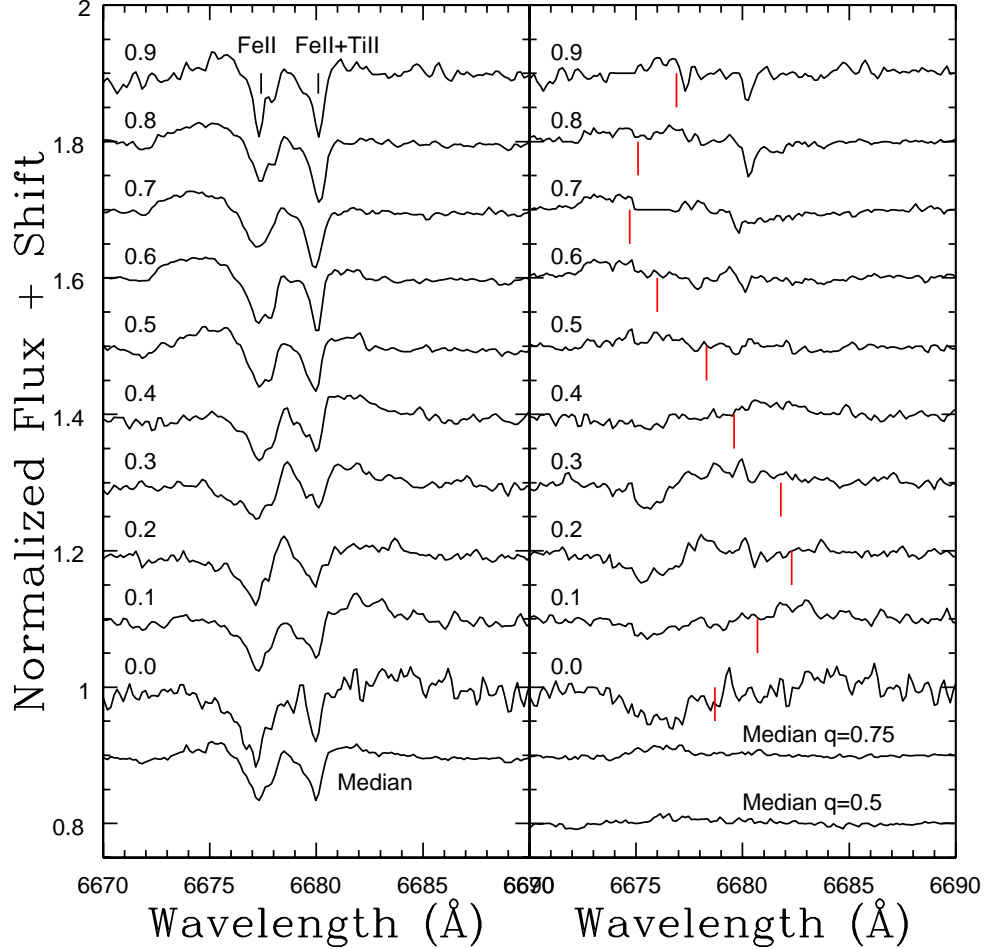


Fig. 12.— Left hand panel: Spectra centered on HeI 6678. The median of spectra in all ten phase bins is shown at the bottom of the panel. Shell lines of FeII and TiII dominate at these wavelengths. Right hand panel: Residuals after subtracting the median spectrum from each spectrum in the left hand column. The red lines mark the expected location of HeI 6678 based on the velocity measurements made by Tarasov & Berdyugin. Emission at a wavelength close to that of HeI 6678 in the restframe is seen in the residual spectra at phase 0.0. This feature is also clearly seen in the phase 0.0 spectrum in the left hand panel. The median residual spectra after shifting spectra into the rest frame assuming mass ratios $q=0.5$ (i.e. that calculated by Tarasov & Berdyugin) and 0.75 are shown at the bottom of the panel. The featureless nature of the combined spectra indicates that HeI 6678 is not detected throughout the entire orbital cycle.

of their more massive brethren (e.g. Kruckow et al. 2018). Van Rensbergen et al. (2011) find that the inclusion of mass and angular momentum loss in their models improves the agreement with the observed period distributions of Algols.

Deschamps et al. (2015) model the IR properties of Algols that are in the early stages of mass transfer. Material is ejected from the system via a wind that originates in a hot spot that forms on the accretion disk. The ejected material cools as it expands outwards, and grains form in their baseline model at a distance of 212 AU from the system. A cloud of moderately hot grains spread over a large volume results. Their models indicate that IR emission from the cloud may be detected with moderate-sized space-based telescopes over angular scales of many arcsec if observed at a distance of 300 pc.

Excess IR emission from V367 Cyg was first noted by Taranova (1997), and entries in the WISE (Wright et al. 2010) point source catalogue at the IRSA ¹ confirm that V367 Cyg is very bright at wavelengths out to at least $22\mu\text{m}$ (i.e. the central wavelength of the W4 filter). Deschamps et al. (2015) note that V367 Cyg is not a point source in WISE images, with the most statistically significant deviation from a point source occurring in the W2 filter ($\lambda_{cen} \sim 4.5\mu\text{m}$).

We have examined the morphology of the V367 Cyg envelope using W2 images that were downloaded from the WISE all-sky survey ². The angular resolution of stars in the W2 image is ~ 9 arcsec FWHM, which corresponds to a spatial resolution of ~ 6000 AU at the distance of V367 Cyg. The W2 image of V367 Cyg is compared with images of two stars that are in the same WISE image tile in Figure 13, and it is clear that V367 Cyg is not a point source.

The envelope around V367 Cyg is not flattened, even though the system is eclipsing, and so is viewed at an oblique angle. If the emission were restricted to a disk with an inclination of 80° , as found from some light curve solutions (e.g. Zola & Ogloza 2001), then the image would be flattened by $\sim 2 : 1$ after factoring in the angular resolution of the W2 images, which is clearly not the case. Taken at face value, the more-or-less round isophotes in Figure 13 suggest that the ejected material flares out over a larger volume than that defined by the orbital plane.

A caveat when investigating the morphology of the environment around V367 Cyg is that there is at least one moderately bright companion, and sub-structure is evident in the W2 image. Still, efforts to model the light distribution in Figure 13 as a collection of

¹https://wise2.ipac.caltech.edu/docs/release/allsky/src_cat

²<https://irsa.ipac.caltech.edu/applications/wise/>

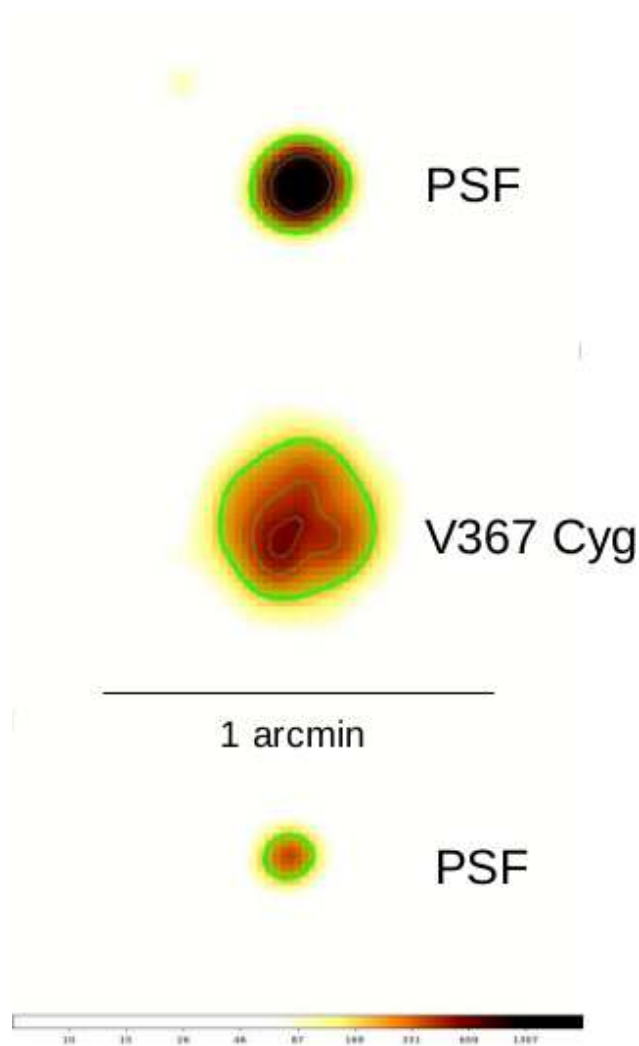


Fig. 13.— W2 images of V367 Cyg and two stars in the same WISE image tile. All images are displayed with the same brightness stretch. The V367 Cyg isophotes are not flattened, suggesting that the emitting material is not confined to a disk. The FWHM of the stellar images is ~ 9 arcsec. V367 Cyg is not a point source, and there are localized peaks in the light distribution that may be companion stars. However, point sources alone can not account for the angular extent of the light distribution at $4.5\mu\text{m}$.

multiple point sources proved unsuccessful – a diffuse background component centered on the system that has almost half of the signal level per pixel of the brightest source in Figure 13 is required to reproduce the extended nature of the W2 light distribution. Thus, while companions may be present, they can not explain the full extent of the light distribution at $4.5\mu\text{m}$.

More quantifiable insights into the spatial extent of emission at $4.5\mu\text{m}$ can be gleaned from the light profile. Figure 14 shows the light profile through the middle column of V367 Cyg in Figure 13 along with the light profile of the PSF constructed from stellar images. Each profile has been normalized to its peak intensity. The V367 Cyg profile has a FWHM of almost 30 arcsec, as opposed to 9 arcsec for the PSF. After removing in quadrature the broadening produced by the PSF, then the intrinsic width of the W2 profile is 28 arcsec. This corresponds to 0.09 parsecs (19000 AU) if the GAIA-based distance of 670 parsecs is adopted. Given the more-or-less symmetric shape of V367 Cyg in Figure 13, then selecting a different orientation for extracting a light profile should not yield a markedly different angular extent. Extended emission at $4.5\mu\text{m}$ around V367 Cyg thus extends over spatial scales of at least a few percent of a parsec.

8. SUMMARY & DISCUSSION

Spectra that cover the wavelength interval $6320 - 6900\text{\AA}$ with a resolution $\frac{\lambda}{\Delta\lambda} \sim 17000$ have been used to examine the CBS V367 Cyg and its surroundings. This wavelength interval has not been extensively observed in past studies of this system. The spectra were recorded over a 7 month time span in 2021, and thus cover roughly 11 orbital cycles.

The observational characteristics of V367 Cyg suggest that it is a W Serpentis system, and so is likely undergoing the initial transfer of mass from the more evolved (and currently more massive) star to its companion. Van Rensbergen et al. (2011) model the orbital periods and mass ratio distributions of CBSs that contain a donor star that is initially spectral type B (i.e. a few solar masses), which is consistent with some of the mass estimates for V367 Cyg. The rate of mass transfer in their models increases towards longer orbital periods, since the donor star must be more evolved as the period increases in order for mass transfer to be initiated. These models predict that systems with orbital periods in excess of 15 days will likely experience Case B mass transfer (i.e. the donor star has evolved off of the main sequence). To the extent that these models hold for V367 Cyg then it is likely that it is undergoing Case B mass transfer, and this is consistent with the spectroscopic characteristics of the donor star (Section 5).

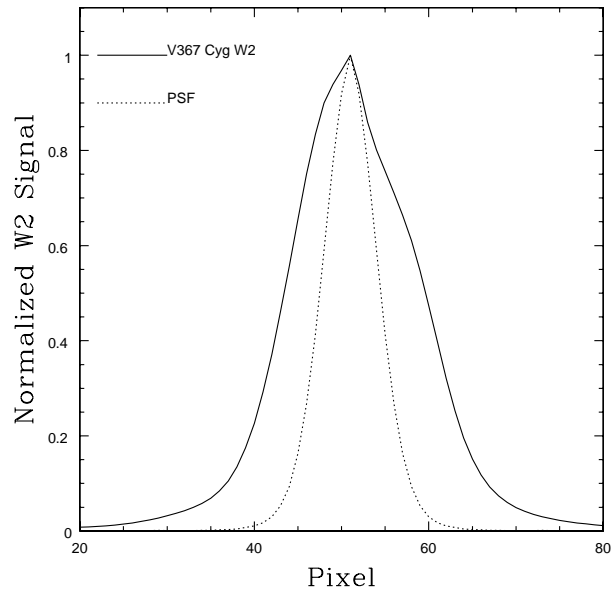


Fig. 14.— Light profiles of V367 Cyg (solid line) and the PSF (dotted line) in the W2 filter. The profiles have been normalized to their peak values, and each pixel along the x axis subtends 1.5 arcsec. The V367 Cyg profile is that of the central column that passes through the image in Figure 13. The V367 Cyg light profile is wider than that of the PSF, and this can not be explained by multiple point sources (see text). Rather, there appears to be emitting material in the W2 image that is spread out over ~ 19000 AU around V367 Cyg.

The deep and narrow absorption features that dominate the red spectrum originate in a circumsystem shell. There are sub-structures in the shell lines that change with orbital phase and time, although in Section 4 it is shown that there is a dominant absorption component in the shell lines that was more-or-less stable with time during the 2021 observing season. Given that the shell almost certainly rotates, then this stability with time suggests that the main body of the shell has uniform structure, in agreement with models that predict that circumstellar material around mass-losing binary systems should be well mixed (e.g. Bermudez-Bustamante et al. 2020).

Evidence is also presented in Section 4 that diffuse absorption lines that originate in the donor star spectrum are embedded in the much stronger shell lines, and that these lines likely have affected efforts to examine the dynamics of the circumsystem shell, in the sense that velocity measurements made from the shell lines have been skewed by contamination from the donor star spectrum. Previous studies have found that velocities measured from the shell lines define a radial velocity curve that is consistent with motion in the same direction as the donor star, but with an amplitude that is considerably smaller. However, the radial velocity curve constructed from a cross-correlation analysis of shell lines that is sensitive to the deepest parts of the strongest shell lines has an amplitude that is smaller than that found in previous studies. Moreover, velocities measured from only the deepest parts of the SiII 6347 and FeII 6432 shell lines, which is the part of the lines where contamination from the donor spectrum should least affect the velocity measurements, have an even smaller amplitude. We emphasize that the shell is likely rotating, but that it does not contain structures that affect the locations of line centers.

The spectrum of the donor star has been extracted by shifting spectra with the shell lines removed into the restframe as defined by the orbital motion of the donor star and then combining the results. The mean spectrum has SiII and FeII absorption lines between 6300 and 6500Å that are slightly weaker in strength than those in the spectrum of the A-type supergiant Deneb. This is consistent with V367 Cyg undergoing Case B mass transfer. The widths of the SiII 6347 line in the donor star spectrum indicate a rotation velocity of $v \sin i \sim 54$ km/sec, in agreement with earlier measurements made from MgII 4481. This rotation velocity is consistent with the donor star being tidally locked for some of the system geometries found by Zola & Ogloza (2001).

There is also evidence that the effective temperature across the face of the donor star varies with orbital phase, in the sense that SiII and FeII lines at phases 0.25 and 0.75 have different depths. Evidence for similar variations in the depth of metallic lines has been seen in previous studies at shorter wavelengths. That this difference in line strength occurs between phases 0.25 and 0.75 is not consistent with gravity darkening, leading us to suspect that

there is large scale spot activity on the donor star. That this behaviour has been evident over $\sim 50+$ years further suggests that the temperature difference between hemispheres has been in place for at least 1000 orbital cycles. This is consistent with the donor star being tidally locked, as suggested by its rotational velocity and some system geometries. Future observations of features such as Ca H and K or HeI $1.058\mu\text{m}$ would be useful to examine the nature of any spot activity on the donor.

Given the success in extracting the spectrum of the donor star, an effort was also made to extract a spectrum associated with the accreting star. Shell-subtracted spectra were shifted into the rest frame using velocities that are appropriate for the accretor after assuming various system mass ratios. The results for each mass ratio were combined, and spectra constructed for mass ratios of unity and 0.75 contain emission features that are attributed to an accretion disk. These lines are formed from the emission components that are seen in the shoulders of metallic absorption lines. We caution that the emission lines in the resulting spectrum are weaker than their actual values, as the technique used to remove shell absorption lines suppresses signal from the emission line centers.

The emission spectra constructed in this manner are similar in some respects to those seen in Herbig AeBe stars, and these objects have the potential to serve as an interpretive guide for understanding the emission spectrum of V367 Cyg. We emphasize that these observational similarities do not mean that we interpret the stars in V367 Cyg as young, forming objects. Rather, it is a pragmatic recognition that the physics of accretion activity in CBSs may produce observational similarities to other astrophysical objects in which accretions disks surround early-type stars – in this case Herbig AeBe stars.

It is perhaps not surprising that $\text{H}\alpha$ is by far the strongest feature in our spectra, appearing as a broad emission feature with deep central absorption. $\text{H}\alpha$ emission in CBSs is associated with interactions between the components, and simulations suggest that it should grow progressively in strength from Case A to Case C mass exchange as the mass flow increases (Deschamps et al. 2015). Previous studies have suggested that the donor star spectrum contributes detectable signatures in higher order Balmer lines. However, comparisons with the spectrum of Deneb indicate that only a very small fraction of the $\text{H}\alpha$ absorption can be attributed to the donor. Unlike was the case for shell lines, the donor star spectrum thus does not skew the $\text{H}\alpha$ profile.

The structure and strength of $\text{H}\alpha$ in the V367 Cyg spectrum changes with both time and orbital phase. The variations in strength with phase are in the sense that absorption and emission are most pronounced during the eclipses, suggesting a possible connection with the L2 and L3 points. The deep central absorption makes it difficult to estimate radial velocities or velocity dispersions for the emission component, although the residuals in the right hand

column of Figure 9 at phases outside of eclipse suggest that the emission moves in a manner that is consistent with the motion of the donor star. As for the absorption component, we speculate that structure in $H\alpha$ absorption might be due to discrete structures along the line of sight, such as might be expected if there is a tightly wrapped spiral outflow. Modelling of such an outflow would be of interest to see if it can replicate the behaviour of $H\alpha$ absorption in these spectra.

[OI] 6364 emission has been detected at all orbital phases. The detection of [OI] emission is perhaps not surprising given its presence in other accretion environments, such as Herbig AeBe stars. [OI] emission in Herbig AeBe stars is correlated with UV flux (Acke et al. 2005), which is a defining characteristic of W Ser systems. [OI] emission also tends to be seen in Herbig AeBe stars that have an IR excess related to circumstellar emission (Viera et al. 2003; Acke et al. 2005), and excess IR emission is another common characteristic of W Ser stars. It would be of interest to survey the spectra of other W Ser systems to examine if there is a correlation between [OI] emission and UV flux and/or the presence of an IR excess.

The [OI] 6364 feature is structurally complex, and has a shape that changes with orbital phase. The shape of the [OI] 6364 emission feature leads us to suspect that a large fraction of the flux is associated with the accretion disk, paralleling the interpretation of [OI] emission in the spectra of Herbig AeBe stars (e.g. Acke et al. 2005). [OI] 6364 should be accompanied by the much stronger [OI] 6300 line, which falls at the blue end of our wavelength coverage. Spectra that sample 6300\AA would be of interest to further characterize [OI] emission and probe conditions in the emitting region.

The spectra have also been used to search for HeI 6678 emission, which might be expected given that it is seen in the model spectra of binary systems undergoing rapid mass transfer generated by Deschamps et al. (2015). This being said, we do not find evidence of HeI emission over a wide range of orbital phases, contrary to what was found by Tarasov & Berdyugin (1998). Rather, there is evidence for HeI emission only near primary minimum, suggesting that the emitting region is located on the side of the accreting star/disk that points away from the donor star. We caution that this detection is preliminary only given that the phase 0.0 spectrum is based on only one observation. We further note that HeI emission line might occur at different orbital phases in the future if the orientation of the excitation source in the system changes.

What conclusions can be drawn about the future of V367 Cyg? An obvious problem is that the masses of the components are not firmly established. Still, while masses are at present uncertain, it might be possible to obtain an upper limit to the mass of the donor based on the environment around the system. Some of the mass estimates for the donor

indicate that V367 Cyg may have formed within the past $\sim 10 - 20$ Myr. Given the rate at which star clusters are disrupted (e.g. Fall and Chandar 2012) then remnants of a star cluster might be found around the system. If such a remnant component could be identified through - say - proper motion and/or parallax measurements then it might be possible to estimate an age for the cluster, and hence a plausible upper mass limit for the donor.

Another source of uncertainty when predicting the future of V367 Cyg is that the system is shedding mass and angular momentum. The material is being fed into the surrounding ISM, with a dust envelope extending over at least 0.09 parsec. The non-conservative nature of the mass transfer complicates efforts to predict the future characteristics of the system given the uncertainties introduced by mass and angular momentum loss (e.g. Yakut & Eggleton 2005). These uncertainties notwithstanding, we suspect that V367 Cyg will evolve into a conventional Algol system after mass reversal, and the ensuing drop in the mass transfer rate. The mass transfer rate estimated by Zola & Ogloza (2001) suggests that the mass ratio might reverse on time scales of $< 10^5$ years if the lower mass estimates for the component stars in Table 1 are correct. The dust envelope is expected to dissipate once rapid mass transfer ends (Deschamps et al. 2015).

We close by noting that the observations discussed here were recorded over only a few orbital cycles, and so provide a snap shot of the system in 2021. The evidence for large scale mass transfer and a circumsystem shell suggest that V367 Cyg is almost certainly in a rapid phase of its evolution, and so large-scale, transient changes in the observational characteristics of the system might occur over short timescales. Hints that this is happening are seen in the $H\alpha$ flux variations discussed in Section 5, as well as the photometric variations in the light curve.

Given the dynamic nature of the observational properties at the present day, longer term monitoring of V367 Cyg will undoubtedly prove to be rewarding, as it will provide a broader perspective of the nature of this system during a defining stage of its evolution. Obtaining spectra with a higher spectral resolution would be of particular interest to better decouple the various components that have been identified in this and earlier papers. This might in turn allow material around the accreting star to be detected throughout the full orbital cycle, raising the possibility of finding reliable masses for both components.

It is a pleasure to thank David Bohlender for reducing the spectra used in this paper. Thanks are also extended to Dmitry Monin for his tireless efforts configuring the DAO telescopes for these (and other) observing programs. This research has made use of the NASA/IPAC Infrared Science Archive (<https://doi.org/10.26131/irsa22>), which is funded by the National Aeronautics and Space Administration and operated by the California Institute

of Technology.

A. Shell Velocity Measurements

The shell velocities used to construct Figure 5 are listed in Table A1. The estimated uncertainty in these measurements is ± 1 km/sec.

Phase	X-Corr ^a	SiII 6347 ^a	FeII 6432 ^a	H α ^b
0.0	-3.3	-10.3	-5.1	-3.7
0.1	-4.5	-7.0	-7.0	-2.3
0.2	-5.7	-9.3	-7.9	-3.2
0.3	-10.0	-8.4	-5.6	0.9
0.4	-8.3	-6.5	-6.5	-1.4
0.5	0.8	-5.5	-6.1	-5.5
0.6	6.4	-1.3	-2.8	-3.7
0.7	3.8	0.1	-5.1	-10.1
0.8	7.3	-0.3	0.5	-3.2
0.9	6.5	-0.8	-2.3	-2.3

Table 3: Shell Line and H α Velocity Measurements

^aVelocities of shell lines, in km/sec, measured from phase-binned spectra using the procedures discussed in Section 4.

^bVelocities of H α absorption, in km/sec, measured from phase-binned spectra using the procedures discussed in Section 6.

REFERENCES

- Abt, H. A. 1954, PASP, 66, 171
- Abt, H. A. 1983, ARAA, 21, 343
- Acke, B., van der Ancker, M. E., & Dullemond, C. P. 2005, A&A, 436, 209
- Aydin, C., Hack, M., & Yilmaz, N. 1978, ApSS, 53, 345
- Bermudez-Bustamante, L. C., Garcia-Segura, G., Steffen, W., & Sabin, L. 2020, MNRAS, 493, 2606
- Bohm, T., & Catala, C. 1994, A&A, 290, 167
- Brown, A. G. A., Vallenari, A., Prusti, T., et al. 2018, A&A, 616, A1
- Clark, J. S., Bartlett, E. S., Coe, M. J., et al. 2013, A&A, 560, A10
- Corcoran, M., & Ray, T. P. 1997, AA, 321, 189
- Davidge, T. J., & Milone, E. F. 1984, ApJS, 55, 571
- Davidge, T. J., & Forbes, D. 1988, MNRAS, 235, 797
- de Mink, S. E., Sana, H., Langer, N., Izzard, R. G., & Schneider, F. R. N. 2014, ApJ, 782, 7
- Deschamps, R., Braun, K., Jurissen, A., Siess, L., Baes, M., & Camps, P. 2015, A&A, 577, A55
- Elias, N. M. II 1990, ApJ, 352, 300
- Ertl, T., Woosley, S. E., Sukhbold, T., & Janka, H.-T. 2020, ApJ, 890, 51
- Fall, S. M., & Chandar, C. 2012, ApJ, 752, 96
- Griffin, R. F., & Griffin, R. 1979, A Photometric Atlas of the Spectrum of Procyon (Cambridge: Cambridge Press)
- Hack, M., Engin, S., & Yilmaz, N. 1984, A&A, 131, 147
- Hamuy, H., Walker, A. F., Suntzeff, N. B., Gigoux, P., Heathcote, S. R., & Phillips, M. M. 1992, PASP, 104, 533
- Heiser, A. M. 1961, ApJ, 134, 568
- Hernandez, J., Calvet, N., Briceno, C., Hartmann, L., & Berlind, P. 2004, AJ, 127, 1682
- Kruckow, M. U., Tauris, T. M., Langer, N., Kramer, M., & Izzard, R. G. 2018, MNRAS, 481, 1908
- Li, Y.-F., & Leung, K.-C. 1987, ApJ, 313, 801
- Lindgren, L. et al. 2018, A&A, 616, A2

- Lloyd, C. 2018, British Astronomical Association Variable Star Section Circular #476, 29
- Malkov, O. Y. 2020, MNRAS, 491, 5489
- Mathew, B. & Subramaniam, A. 2011, BASI, 39, 517
- McAlister, H. A., & Hattkopf, W. I. 1988, The Second Catalogue of Interferometric Measurements of Binary Stars (Atlanta: Georgia State University Press), 117
- Milone, E. F. 1968, AJ, 73, 708
- Monin, D., Saddlemyer, L., Bohlender, D. 2014, RevMex, 45, 69
- Nelson, C. A., & Eggleton, P. P. 2001, ApJ, 552, 664
- O’Connell, D. J. K. 1951, Pub. Riverview College Obs., 2, 85
- Pavlovski, K., Schneider, H., & Akan. M. C. 1992, A&A, 258, 329
- Plavec, M. J., & Koch, R. H. 1978, IBVS, 1482
- Plavec, M. J., Dobias, J. J., Etzel, P. B., & Weiland, J. L. 1984, NASCP, 2349, 420
- Reipurth, B., Pedrosa, A., & Lago, M. T. V. T. 1996, A&AS, 120, 229
- Roman, N. G. 1956, ApJ, 123, 246
- Sahman, D. I., Dhillon, V. S., Marsh, T. R., Moll, S., Thoroughgood, T. D., Watson, C. A., & Littlefair, C. A. 2013, MNRAS, 433, 1588
- Sana, H., de Mink, S. E., de Koter, A. et al. 2012, Sci, 337, 444
- Schneider, H., Pavlovski, K., Planinic, M., & Ivezić, Z. 1993, A&A, 277, 480
- Simon, M. 1997, ApJ, 482, L81
- Smith, N., & Tombleson, R. 2015, MNRAS, 447, 598
- Taranova, O. G. 1997, Ast. Lett., 23, 704
- Taranova, O. G., & Shenavrin, V. I. 2005, Ast. Lett., 31, 598
- Tarasov, A. E., & Berdyugin, A. V. 1998, Astron. Rep., 42, 494
- Van Rensbergen, W., De Greve, J. P., Mennekens, N., Jansen, K., & De Loore, C. 2011, A&A, 528, A16
- Viera, S. L. A., Corradi, W. J. B., Alencar, S. H. P., et al. 2003, AJ, 126, 2971
- Wilson, R. E. 1981, ApJ, 251, 246
- Wilson, R. E. 2018, ApJ, 869, 19
- Wright, E. L., Eisenhart, P. R. M., Mainzer, A. K., et al. 2010, AJ, 140, 1868
- Zhao, M., Gies, D., Monnier, J. D., et al. 2008, ApJ, 684, L95

Zola, S., & Ogloza, W. 2001, A&A, 368, 932